CALIBRATION OF A RADIOBIOLOGICAL IRRADIATOR: THE FAXITRON CABINET X-RAY SYSTEM MODEL CP160

by

Ismail AlDahlawi
Medical Physics Unit
McGill University, Montreal
January 2008

A thesis submitted to the Faculty of Graduate Studies and Research
in partial fulfillment of the requirements of the degree of
Master of Science in Medical Radiation Physics

Your file Votre référence
ISBN: 978-0-494-51059-9
Our file Notre référence
ISBN: 978-0-494-51059-9

ABSTRACT

Radiobiological irradiation can be performed using appropriately collimated sealed source radioisotope machines such as Co-60 units, as well with X-ray tubes and linear accelerators. The increasing research interest in delivering organ-specific or whole body animal external irradiation has led to the introduction of dedicated X-ray units for research purposes. In this work, the proprieties of a kilovoltage X-ray biological irradiator, the Faxitron cabinet X-ray system model CP160, are investigated and dosimetrically characterized. Calculation formalisms for everyday use of the radiobiological irradiator in laboratory conditions, specifically for cell cultures and small animals total body irradiation, were developed following the AAPM TG-61 protocol. The quality of the X-ray beams generated by this irradiator was found to range between HVL 0.7 mm Cu for a 160 kVp 0.5 mm Cu filtered beam, and HVL 0.07 mm Al for a 20 kVp non-filtered beam. Our calculation formalisms for cell cultures and small animal irradiations were found to be valid within ±5%.

RÉSUMÉ

L'irradiation radiobiologique peut être effectuée à l'aide de machines à source radioisotopique celée et collimatée de manière appropriée, telles que les unités au ^{60}Co, ou à l'aide de tubes à rayons X et d'accélérateurs linéaires. L'intérêt croissant pour la recherche sur l'irradiation d'organes spécifiques ou de corps entiers d'animaux a mené à l'introduction d'unités à rayons X dédiées à la recherche. Dans ce travail, les propriétés d'un irradiateur biologique à rayons X en kilovoltage, l'armoire à rayons X Faxitron modèle CP160, ont été étudiées et la dosimétrie de l'irradiateur a été décrite. Des formalismes de calcul pour l'usage quotidien de l'irradiateur radiobiologique en conditions de laboratoire ont été développés suivant le protocole de l'AAPM TG-61, spécifiquement pour l'irradiation de cultures cellulaires et de petits animaux. Nous avons trouvé que la qualité des faisceaux de rayons X générés par cet irradiateur est dans un intervalle allant d'une CDA de 0,7 mm Cu pour un faisceau de 160 kVp filtré avec 0,5 mm Cu, à une CDA de 0,07 mm Al pour un faisceau de 20 kVp non filtré. Nos formalismes pour l'irradiation de cultures cellulaires et de petits animaux dévient des mesures avec des erreurs relatives inférieures à ±5 %.

ACKNOWLEDGMENTS

I would like to express my gratitude to both my supervisors, *William Parker* and Dr. *Jan Seuntjens*, for their guidance, support and patient throughout the completion of this work.

I would also like to thank the entire Medical Physics staff who are always eager to help. In particular, *Michael Evans*, *Micheline Gosselin* and Dr. *Gyorgy Hegyi* for their supply with some of the tools I needed to do this work. I am grateful for the help given by Eng. *Pierre Léger* with some of the technical difficulties I faced with the machine, and for all the shop work done by *Robin Van Gils*. Many thanks to *Horacio J. Patrocinio*, Dr. *Wamied Abdel-Rahman*, and Dr. *Slobodan Devic* for their discussions and advice.

Last but not least, I would like to thank Dr. *Ervin Podgorsak* for giving me the great opportunity to major in this rewarding field in an environment with such a high standard of teaching and research.

This thesis is dedicated to my mother, *Bahiyah Dahlawi*, who passed away before seeing me a McGill graduate, and to my father, *Abdulmajeed AlDahlawi*, both for their infinite love and support.

TABLE OF CONTENTS

CHAPTER 5

RESULTS AND DISCUSSION

LIST OF FIGURES

LIST OF TABLES

CHAPTER 1

INTRODUCTION

This chapter provides an introduction to radiobiological irradiators and some basic radiation biology concepts, and also discusses the protocols for kilovoltage beam dosimetry and the British Journal of Radiology (BJR) supplements. The chapter concludes with stating the aims and goals of the work described in this thesis.

1.1 Introduction to Radiobiological Irradiators

Radiobiological irradiation has been performed using appropriately collimated sealed source radioisotope machines such as Co-60 units, as well with X-ray tubes and linear accelerators. The increasing research interest in delivering organ-specific or whole body animal external irradiation has led to the introduction of dedicated X-ray units for research purposes. Advantages of the latter include less stringent facility-licensing requirements, more accessibility, lower costs, smaller equipment size, and easier maintenance. In addition, a dedicated radiation unit for experimental work is preferable because infection control practices within large animal facilities can often prevent the transfer of animals between the animal colony and a remotely located irradiator.

In this project, a commercially available X-ray radiobiological irradiator, Faxitron model CP160 (Faxitron X-Ray Corp., Wheeling, IL, USA), is investigated and its radiation properties are characterized.

1.2 Radiation Biology

Radiation biology is a branch of science concerned with the action of ionizing radiation on biological tissues and living organisms. Radiobiology is a combination of three disciplines: radiation physics, chemistry and biology. All living things are made up of cells, which contain inorganic compounds (water and minerals) as well as organic compounds (proteins, carbohydrates, nucleic acids and lipids). Two main parts of a cell are the cytoplasm, which supports the metabolic function, and the nucleus, which contains the genetic information (DNA). Ionizing radiations, such as X-rays, interact with matter creating charged particles in motion, which, in turn, interact and deposit their energy in matter as a result of coulomb interactions. The average energy lost by a particle over a given track length is known as the linear energy transfer (LET). The units of LET are given in terms of energy lost per unit path length (e.g., keV/μm).[1] LET is an indicator of the efficiency with which different types of ionizing radiation causes biological damage, and is used in radiobiology for defining the quality of an ionizing radiation beam. Table 1-1 shows typical values for commonly used radiations.

Radiation	LET (keV/μm)
Photons	
250 kVp	2
Co-60 (1.25 MeV)	0.3
3 MeV	0.3
Electrons	
10 keV	2.3
100 keV	0.5
1 MeV	0.25
Charged Particles	
Proton 2 MeV	17
Alpha particles 5 MeV	90
Carbon Ion 100 MeV	160
Neutrons	
14 MeV	12

Table 1-1 Linear Energy Transfer (LET) of various radiation.[1,2]

When cells are exposed to ionizing radiation, the standard physical effects between radiation and the atoms or molecules of the cells occur first, followed by possible biological damage to cell function. The biological effects of radiation result mainly from damage to DNA. However, there are also other sites in the cell that may lead to cell death when damaged. The damage to the cell due to radiation may occur in two ways: direct action, where the radiation interacts directly with the critical target in the cell; or indirect action, where the radiation interacts with a neighbouring molecule (mainly water) within the cell to produce free radicals (e.g. water ion: H_2O^+, and hydroxyl radical: $OH^\bullet$) which, in turn, can interact chemically with other molecules causing damage to a critical target within the cell. Direct action is the dominant process in the

interaction of high LET particles; and for low LET radiation, about two thirds of the biological damage is due to indirect action.

The effect of radiation on the human population can be classified as either somatic, which are effects that exposed individuals suffer during their lifetime, such as radiation induced cancer, sterility, opacification of the eye lens and life shortening; or genetic (hereditary) effects, which affects an individual's genes and DNA that can contribute to the birth of defective descendants.

The effects of radiation may be further classified into two categories: stochastic and deterministic (non-stochastic). In stochastic effects, the probability of occurrence increases with increasing dose, but the severity in affected individuals does not depend on the dose. There is no threshold dose for this type of effect. Examples include induction of cancer and genetic effects. Deterministic effects, on the other hand, increase in severity with increasing dose and have a threshold dose. Examples of deterministic effects are organ dysfunction, fibrosis, lens opacification, blood changes and decreases in sperm count.

An organ or tissue can express response to radiation damage in either an acute effect, i.e., soon after exposure to radiation, such as inflammation, oedema, haemorrhage; or as a late effect , i.e., delayed after exposure to radiation, such as atrophy, fibrosis and obstruction of the intestine.

The experiments carried out using the radiobiological irradiator characterized in this thesis are performed on samples of cell cultures or small animals like mice. The irradiations are performed as whole body irradiations with doses ranging between 1 to 10 Gy. For our experiments, the dose accuracy needed is ±5% of the prescribed dose with a

±10% uniformity within the cells/mice volume in accordance to the European Late Effects Project Group (EULEP) protocol for X-ray dosimetry in radiobiology.[3]

1.3 Protocols for Kilovoltage Beam Dosimetry

The development of dosimetry for kilovoltage X-ray beams (low and medium energy < 400 kV) remained more or less static between the 1960s and 1980s. The International Atomic Energy Agency published a protocol in 1987, referred to as IAEA (1987) Code of Practice TRS 277[4], that devoted a detailed section to kilovoltage X-rays. The protocol used a new air kerma quantity, rather than the old unit of exposure based on the Roentgen. TRS 277 also used new Monte Carlo generated backscatter factors, and chamber perturbation factors for the medium-energy in-phantom measurements.[5] The "air kerma" formalism has been followed by several national dosimetry protocols on kilovoltage X-ray dosimetry such as the IPEMB 1996 protocol[6] in UK, NCS 1997 protocol[7] in the Netherlands and Belgium, and the North American protocol followed in this work, the AAPM TG-61.[8]

The air kerma based in-phantom calibration method, referred to as the In-Phantom method in AAPM TG-61 protocol, is used mainly for medium energy X-ray beams, typically ranging between 100 and 300 kV. Various dosimetry protocols recommend that the dose be determined at a depth in a water phantom, but they differ in their specifications of the reference depth. Both TRS 277 and ICRU 23[9] specify a depth of 5 cm, while the TRS 398[10] (the successor of TRS 277), the IPEMB 1996 and the AAPM TG-61 specify a depth of 2 cm in water for the reference depth, considering this to be

mush more representative of clinical practice. In general, cylindrical chambers of the Farmer type are used at this energy range.

For low and medium (40-100 kV) photon beam energies, the air kerma based backscatter method, referred to as the In-Air method in AAPM TG-61, is typically used. Clinically, for these beams, the dose is most often prescribed at the skin surface. In this method, the chamber is positioned in air (i.e., with no phantom involved) at a position corresponding to the centre of the field on the patient's skin surface. This is then converted into dose to water at the surface of a phantom at the field size of interest. The energy or quality range for this method differs slightly from protocol to protocol, but all of the protocols denote it by the term "low energy". The IPEMB protocol recommends that a cylindrical chamber is to be used over the complete medium and low energy range, while both the TRS 398 and AAPM TG-61 protocols recommend the use of a parallel plate chamber for the low energies (X-ray tube energies approx. below 70 kV), and a cylindrical chamber for the medium energies (higher than 70 kV).

For very low photon energies (8-50 kV), methods described in the German[11] and UK (IPEMB) protocols can be used. In this energy range a thin window parallel-plate chamber is placed at the surface of a phantom and the dose at the surface is determined.

1.4 BJR Supplements: Central Axis Depth Dose Data for Use in Radiotherapy

The BJR supplements, published by the British Institute of Radiology, provide data for central depth dose for various radiation beams used for radiotherapy. Values of a specific dosimetric parameter were gathered from different centers around the world and

published in various supplements. This includes data on peak scatter factors, percentage depth doses and tissue air ratios for various radiation beams. The supplements are used as a standard reference for expected values that should be obtained when measuring beam parameters of similar radiation beams. The supplements are updated when additional measured dosimetric data become available or when modification of the previous tabulated data are required. The first supplement was BJR Supplement 5 (1953)[12] followed by BJR Supplement 10 (1961)[13], BJR Supplement 11 (1972)[14], BJR Supplement 17 (1983)[15], and the most recent BJR Supplement 25 (1996).[16]

BJR Supplement 17 was released as a revision of BJR Supplement 11 with some expansion. The photon beam data, for example, were extended to include photon energies up to 43 MV. Also the Supplement 17 includes data obtained from a various units manufactured by different companies. As for low energy X-rays beams (0.01 – 8 mm Al HVL, approx. 6 – 150 kVp), minor changes have been made to some of the tables and other tables were replotted.

The most recent BJR supplement, BJR Supplement 25, includes new high energy photon data, updated backscatter factors for low energy X-rays, new neutron data and inclusion, for the first time, of proton data. The new supplement also added a half-value layer conversion formula from aluminium to copper in the energy range of 50-300 kV X-rays. Available data for low energy X-ray depth doses have been reviewed for low energy X-rays beams (0.01 – 8 mm Al HVL, approx. 6 – 150 kVp).

1.5 Purpose of the Thesis

The main objectives of this thesis are to:

- Dosimetrically characterize the X-ray beam generated by the radiobiological irradiator: Faxitron model CP160.
- Develop a calculation formalism for everyday use of the radiobiological irradiator in laboratory conditions, specifically for cell cultures and small animal total body irradiation.

1.6 References

[1] I. Tannock, *The Basic Science of Oncology*, 4th ed. (McGraw-Hill, Medical Pub. Division, New York, 2005).

[2] E. B. Podgorsak (Editor), *Radiation Oncology Physics : A Handbook for Teachers and Students*. (International Atomic Energy Agency, Vienna, 2005).

[3] J. Zoetelief, J. J. Broerse, R. W. Davies et al., "Protocol for X-ray dosimetry in radiobiology", Int J Radiat Biol **77** (7), 817-835 (2001).

[4] P. Andreo, J.C Cunningham, K Hohlfeld et al., *Absorbed dose determination in photon and electron beams: an international code of practice, IAEA Technical Reports Series 277*. (International Atomic Energy Agency, Vienna, 1987).

[5] A. E. Nahum,"kV X-ray Dosimetry: Current Status and Future Challenges (AAPM Proc. no 11)", *in Proceedings of the Kilovoltage X-ray Beam Dosimetry for Radiotherapy and Radiobiology*, edited by C.-M, Ma and Jan P. Seuntjens (Medical Physics Publishing, Madison, Wisconsin, 1998)

[6] S. C. Klevenhagen, R. J. Aukett, R. M. Harrison et al., "The IPEMB code of practice for the determination of absorbed dose for x-rays below 300 kV generating potential (0.035 mm Al-4 mm Cu HVL; 10-300 kV generating potential)", Phys Med Biol **41** (12), 2605-2625 (1996).

[7] NCS (Netherlands Commission on Radiation Dosimetry), *Dosimetry for low and medium energy x-rays: a code of practice in radiotherapy and radiobiology, NCS Report no. 10*. (NCS, Delft, The Netherlands, 1997).

[8] C. M. Ma, C. W. Coffey, L. A. DeWerd et al., "AAPM protocol for 40-300 kV x-ray beam dosimetry in radiotherapy and radiobiology", Med Phys **28** (6), 868-893 (2001).

[9] ICRU (International Commission for Radiation Units and Measurements), *Radiation dosimetry: Measurement of absorbed dose in a phantom irradiated by a single beam of x- or gamma rays, ICRU Report No. 23.* (1973).

[10] P. Andreo, D. T. Burns, K. Hohlfeld et al., *Absorbed Dose Determination in External Beam Radiotherapy: An International Code of Practice for Dosimetry Based on Standards of Absorbed Dose to Water; Technical Reports Series No. 398.* (International Atomic Energy Agency, Vienna, 2000).

[11] DIN (Deutsch Institut Fur Normung), *Klinische Dosimetrie: anwendung von Röntgenstrahlen mit Röhrenspannungen von 100 bis 400 kV in der Strahlentherapie* (DIN, Berlin, 1996).

[12] "Central axis depth dose data for use in radiotherapy, BJR Supplement no. 5", Br. J. Radiol, (1953).

[13] "Central axis depth dose data for use in radiotherapy, BJR Supplement no. 10", Br. J. Radiol, (1961).

[14] "Central axis depth dose data for use in radiotherapy, BJR Supplement no. 11", Br. J. Radiol, (1972).

[15] "Central axis depth dose data for use in radiotherapy, BJR Supplement no. 17", Br. J. Radiol, (1983).

[16] "Central axis depth dose data for use in radiotherapy, BJR Supplement no. 25", Br. J. Radiol, (1996).

CHAPTER 2

RADIATION PHYSICS OF LOW ENERGY PHOTON BEAMS

This chapter presents a review of basic radiation physics concepts concerning photon interactions. The chapter also discusses dose and dose-related concepts and some relevant dosimetric functions.

2.1 Definition of Low and Medium Energy Photon Beam

The term "low energy photon beam" used in this thesis is defined for photon energies ranging between 10 keV and 100 keV, while the term "medium energy photon beam" is defined for photon energies ranging between 100 keV and 300 keV.

2.2 Classification of Photon Radiation

Photon radiation can be classified depending on its origin to four major types:[1]

- Characteristic X-rays: resulting from an electron transmitted from one allowed orbit to a vacancy in another allowed orbit.
- Bremsstrahlung X-rays: resulting from electron-nucleus interactions.
- Gamma rays: resulting from nucleus translation in gamma decay.
- Annihilation radiation: resulting from electron-positron annihilation which yields, typically, two 511 keV photons in opposite directions.

Bremsstrahlung yields a continuous X-ray spectrum, while for the other three types a discrete photon spectrum is emitted. Mostly Bremsstrahlung and Characteristic X-rays are produced when using low energy X-ray tubes. Gamma rays, which are emitted from

radioactive materials, and annihilation radiation, which has a high threshold energy of 1.022 MeV, are not seen in low energy X-ray tube production.

2.3 X-Ray Beam Production

X-ray beams are produced by bombarding a thick high *Z*-material target with a focused electron beam. As electrons interact in the target, photons are produced through two main processes: The first process, bremsstrahlung, where by the incident electron interacts with the nucleus field, resulting in the emission of a photon ranging in energy between zero and the kinetic energy of the incident electron. The second process, characteristic emission, occurs as a result of electron transitions between atomic orbitals following an electron – electron interaction. The resulting photon has a discrete energy equal to the difference in binding energy between the two electron shells involved.

2.4 Interactions of Photons with Matter

As a photon travels inside the material, it interacts with its atoms. For low and medium photon energies (less than 1022 keV in general), there are mainly three types of interactions: Photoelectric effect, Coherent (Rayleigh) scattering, and Incoherent (Compton) scattering.

The photoelectric effect is an interaction between the incident photon and a tightly bound orbital electron. Figure 2-1 illustrates the photoelectric effect interaction. The photon gives all its energy to the electron and disappears, resulting in the ejection of the electron (called photoelectron) from the atom with a kinetic energy, E_k, equivalent to the incident photon energy, $h\nu$, minus the binding energy of the electron, E_b. i.e.,

$$E_k = h\nu - E_b \qquad (2\text{-}1)$$

Following the photoelectric effect we expect atomic relaxation through the emission of Characteristic X-ray or Auger electron emission.

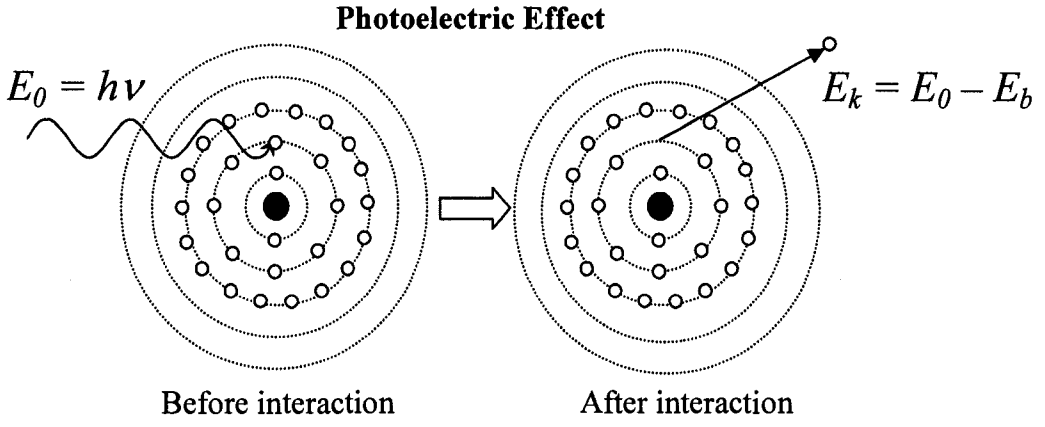

Figure 2-1: Schematic drawing of photoelectric interaction of a photon with a tightly bound electron and the emission of a photoelectron.

In coherent (Rayleigh) scattering, as shown in Figure 2-2, the incident photon also interacts with a bound orbital electron. The photon does not transfer energy to the electron, but the photon's direction is changed.

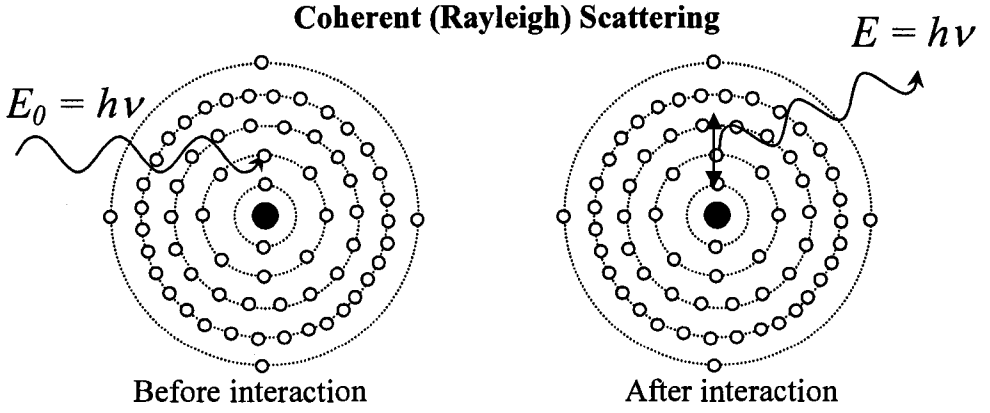

Figure 2-2: Schematic drawing of coherent (Raleigh) scattering of a photon with a bound orbital electron.

Incoherent (Compton) interaction happens when a photon interacts with a "quasi-free" orbital electron. The orbital electron is considered to be quasi-free when the energy of the incident photon is much larger than the binding energy of the electron. A schematic drawing of Compton interaction is shown in Figure 2-3. In this interaction, the photon transfers some of its energy to the electron and undergoes scattering at angle θ with energy $h\nu'$.

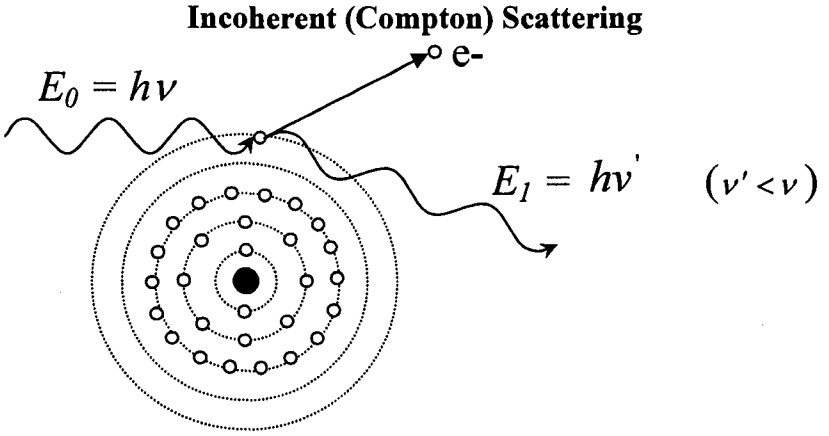

Figure 2-3: Schematic drawing of incoherent (Compton) scattering of a photon with a free electron.

For high energy photon beams (> 1.022 MeV = 2 $m_e c^2$), a pair production interaction is possible, in which a photon disappears in the field of the nucleus giving its energy to produce an electron and positron. In a similar phenomenon called triplet production, a photon disappears in the field of an orbital electron resulting in an electron – positron pair plus the orbital electron. Triplet production requires a photon energy threshold of 2.044 MeV (= 4 $m_e c^2$).

The probability that a single photon undergoes one of these interactions, also referred to as the cross section, depends on the energy $h\nu$ of the photon and the atomic number Z of the material. A quantity called atomic attenuation coefficient describes this

probability. Atomic attenuation coefficients are often normalized to the density of the material used. For photoelectric effect, the mass attenuation coefficient, noted by τ/ρ, is proportional to $(Z/h\nu)^3$. In addition to the steady decrease of τ/ρ with increasing incident photon energy $h\nu$, sharp peaks are encountered for certain energies corresponding to the binding energy for a specific electronic shell of the material. For coherent (Rayleigh) scattering, the mass cross section, σ_R/ρ, is proportional to $(Z/h\nu^2)$. While for incoherent (Compton) scattering, the mass cross section, σ_C/ρ, is independent of the material atomic number Z since Compton scattering is an interaction between an incident photon and a quasi-free electron. σ_C/ρ also decreases with increasing incident photon energy.[1]

The total mass attenuation coefficient μ/ρ, shown in Figure 2-4 as a function of energy for Lead and Water, is the sum of mass coefficients for the individual photon interactions. In the case of low and medium energy X-ray, μ/ρ is:

$$\mu/\rho = \tau/\rho + \sigma_R/\rho + \sigma_C/\rho \qquad (2\text{-}2)$$

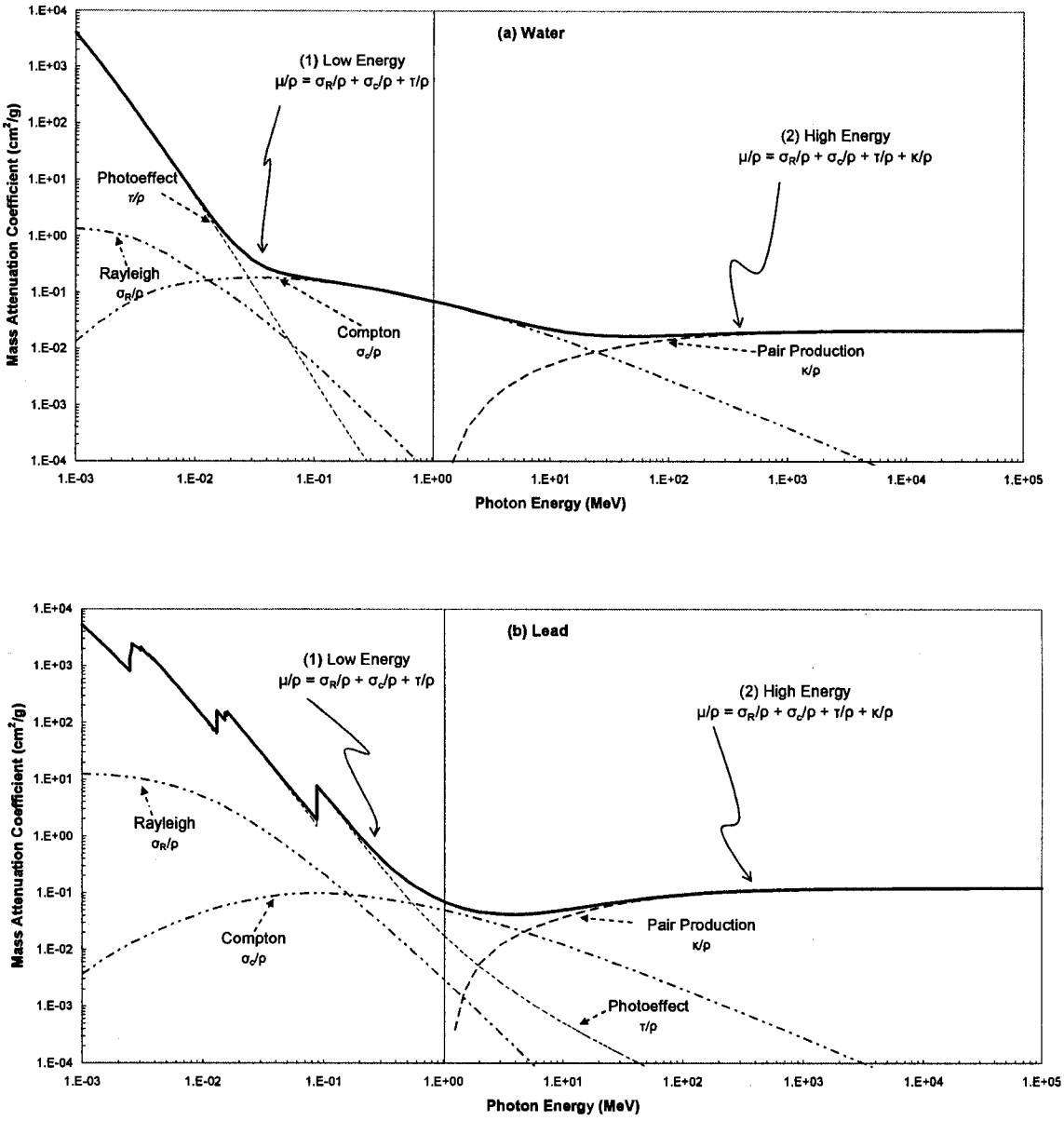

Figure 2-4: Plots of total mass attenuation coefficients for water and lead. The figures also show individual coefficients for each of photoelectric effect, Rayleigh, Compton and pair production interaction.

2.5 Attenuation Law

A narrow monoenergetic photon beam, of initial number of photons N_0, travelling through a material encounters attenuation as some of the photons are absorbed and scattered away. The number of photons, N, that reach a depth x in the material is given by the following "attenuation law":

$$N = N_0 e^{-\mu x} \qquad (2\text{-}3)$$

where μ is the total linear attenuation coefficient of the attenuator.

The quantity $e^{-\mu x}$ is the probability (i.e., N/N_0) that a photon will pass through a slab of thickness x without interacting.[2]

Since the intensity of a photon beam is proportional to the number of photons, the intensity, I, also undergoes attenuation following the attenuation law, i.e.,

$$I = I_0 e^{-\mu x} \qquad (2\text{-}4)$$

2.6 Half-Value Layer and Effective Energy

A special value of the attenuator thickness x, referred to as the half-value layer (*HVL*), is defined as the thickness required to attenuate the intensity of the photon beam by half. Applying *HVL* in the attenuation law equation, Equation (2-4), yields a simple relationship between *HVL* and the total attenuation coefficient:

$$\frac{I}{I_0} = \frac{1}{2} = e^{-\mu HVL} \Rightarrow HVL = \frac{\ln(2)}{\mu} \qquad (2\text{-}5)$$

Tables of the total attenuation coefficients as a function of photon energy are available for different materials.[3]

The second half-value layer, HVL_2, is defined as the thickness required to further attenuate by half the intensity of a beam attenuated by one *HVL*. The ratio of the first *HVL* to the second *HVL* is called the homogeneity coefficient, *HC*. For a monoenergetic beam, the second *HVL* is equal to the first *HVL* and thus the homogeneity coefficient *HC* is equal to 1. However, this is not the case for a low energy beam composed of different photon energies (polyenergetic beam), where the low energy part of the spectrum is preferentially attenuated as the beam passes through material leading to a larger value for the second *HVL* than the first *HVL*, i.e., $HC<1$.

For a photon beam composed of different energy photons (i.e., a spectrum of energy), one can determine an effective energy E_{eff}, defined as the energy of a monoenergetic X-ray beam which has the same *HVL* as the polyenergetic beam. This is done by measuring the *HVL* of that beam, and then finding the attenuation coefficient using Equation (2-5). A lookup table[3] of μ versus energy gives us the value of E_{eff}.

A complete specification of the quality of a photon beam requires the knowledge of its spectrum emitted by the source. However, this is not practical as spectral measurements are not easily performed and thus, in low energy X-ray beams, the peak energy *kVp* and the first half-value layer HVL_1 are often used to characterize a polyenergetic photon beam.[4]

2.7 Inverse square law

A photon beam encounters reduction in its intensity inversely proportional to the square of the distance from the source, *f*, as it propagates through a vacuum or air, i.e., for

two different source distances f_1 and f_2, their corresponding intensities I_1 and I_2 are related using the expression:

$$\frac{I_1}{I_2} = \left(\frac{f_2}{f_1}\right)^2 \qquad (2\text{-}6)$$

This is also true for other quantities such as photon fluence(ϕ), exposure in air (X), air kerma in air $(K_{air})_{air}$, and dose to small mass of medium in air (D'_{med}).

2.8 Radiation Quantities

2.8.1 Exposure

Exposure (X) is a quantity used to describe the output of X-ray tube. It is defined for gamma rays and X-rays as the amount of charge produced as the beam interacts in air per unit mass of air. Exposure is expressed in C/kg, or Roentgen (1 R = 2.58 x 10^{-4} C/kg).[5] The International Commission on Radiological Units and Measurements (ICRU)[6] has defined exposure for energies below 3 MeV as $\frac{dQ}{dm_{air}}$, where dQ is the sum of all charges of one sign produced as photons travel in a mass dm of air.

2.8.2 Kerma

Kerma (K) is an acronym for kinetic energy released in matter. It is defined only for indirectly ionizing radiation (e.g., photons and neutrons). Kerma is defined as the energy transferred from indirectly ionizing radiation to charged particles in the medium per unit mass:

$$K = \frac{d\bar{E}_{tr}}{dm} \qquad (2\text{-}7)$$

with a unit of J/kg, or Gray (Gy) where 1 Gy = 1 J/kg.

Kerma may be subdivided into two categories: collision kerma, K_{col}, resulting from the energy transferred due to collisional interactions, and radiative kerma, K_{rad}, resulting from energy transferred through radiative process (bremsstrahlung and in-flight annihilation).

The collision air kerma and exposure are related through the following relationship:[4]

$$(K_{col})_{air} = \left(0.876 \frac{cGy}{R}\right) X \qquad (2\text{-}8)$$

where the exposure X is expressed in roentgens.

2.8.3 Absorbed Dose

Energy from a photon beam is imparted to the medium in a two step process: first the kinetic energy is transferred from the photon to an electron (i.e., kerma), then the electron deposits some of its kinetic energy into the medium (i.e., absorbed dose). Some of the remaining kinetic energy is lost in the form of radiative losses (bremsstrahlung, in-flight annihilation).

The absorbed dose, D, is defined as the average energy absorbed in the medium per unit mass:

$$D = \frac{d\bar{\varepsilon}}{dm} \qquad (2\text{-}9)$$

with a unit of gray (Gy), where 1 Gy = 1 J/kg.

2.9 Dosimetric Functions

Several dosimetric functions are defined to describe and calculate the dose distribution inside the animal body "tissue" or phantom. The photon beam needs to be calibrated first at a single reference point, usually at the depth of maximum dose, then the dose in medium is related to this calibration point through these dosimetric functions.

Before discussing these functions in more detail, the following parameters, shown schematically in Figure 2-5, need to be defined:

f: X-ray source to surface distance;

z: depth inside the animal body or phantom;

Q: point of interest at depth *z*;

D_Q: dose at point *Q*;

z_{max}: depth of maximum dose inside the animal body or phantom;

P: point at depth z_{max};

D_p: dose at point *P*, it is also the maximum dose;

A: field size at the surface of the animal body or phantom;

A_Q: field size at point *Q* inside the animal body or phantom;

D': Dose to small mass of tissue; small enough not to attenuate the beam, but large enough to satisfy charge particle equilibrium (CPE) condition.

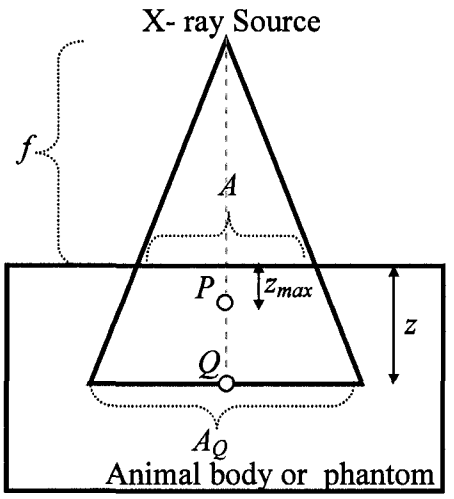

Figure 2-5: Parameters used in dosimetric functions.

2.9.1 Factors Accounting for Change in Dose at a Reference Point: *ISF* and *PSF*

a) Inverse Square Factor (*ISF*)

As discussed previously in Section 2.7, the dose to small mass of tissue in air (D') is inversely proportional to the square of the distance from the source. i.e.,

$$\frac{D_1'}{D_2'} = \left(\frac{f_2}{f_1}\right)^2 \qquad (2\text{-}10)$$

b) Peak Scatter Factor (*PSF*)

Peak Scatter Factor (*PSF*) is the ratio of the total dose to the primary dose at z_{max}:

$$PSF(A_Q, hv) = \frac{D_p(z_{\max}, A_Q, hv)}{D_p'(A_Q, hv)} \qquad (2\text{-}11)$$

For a low energy photon beam, the depth of maximum dose is at the surface, and peak scatter factor in this case is referred to as backscatter factor (*BSF*). Also note in this case the field size A_Q at the point Q $(=P)$ is actually the field size A at the surface.

BSF depends on the field size and beam quality. As the field size becomes larger, *BSF* increases because of the increasing scattering contribution. *BSF* increases for low quality beams reaching a maximum of 1.5 around 0.4 and 0.6 mm Cu HVL and then decreases for higher quality beams.[4,7] *BSF* is also weakly dependent on the distance from the source *f*.[8]

2.9.2 Factors Relating Dose at Depth to Dose at a Reference Point: *PDD*, *TAR*, *TPR* and *TMR*

a) Percentage Depth Dose (*PDD*)

The dose distribution along the central axis inside the animal body or phantom is usually expressed as a percentage normalized to the dose at depth of maximum dose D_p, refer to Figure 2-6 for the setup of *PDD*,

$$PDD(z,A,f,hv) = \frac{D_Q}{D_p} \times 100 \qquad (2\text{-}12)$$

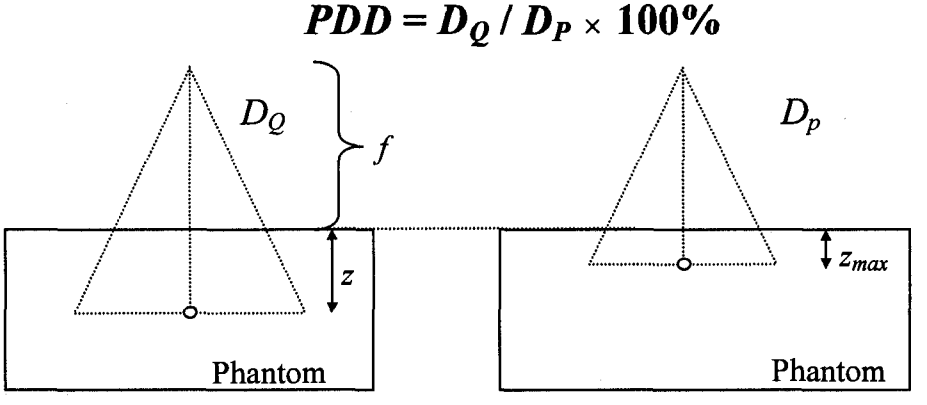

Figure 2-6: Setup for percentage depth dose (PDD) measurements.

For a low energy photon beam, the depth of maximum dose is at the surface. The beam quality *hv*, depth *z*, field size *A*, and source to surface distance *f* are the parameters that influence the central axis depth dose distribution. *PDD* increases with increasing beam quality *hv* since a higher quality beam has more penetrating power. The effect of attenuation law, together with inverse square law and scattering decreases the dose with increasing depth *z*. Increasing the field size *A* results in increasing *PDD* as more scattered photon contribute to the dose. Finally, *PDD* increases with source to surface distance *f* because of the smaller effect of inverse square law as we increase *f*, i.e., the drop of doses between two points is much greater for small source distances than for larger distances resulting in increasing of *PDD* with increasing *f*. Conversion between two *PDD*s, for different source to surface distances, f_1 and f_2, and field sizes. A_1 and A_2, is possible using the equation:[7]

$$\frac{PDD(z, A_1, f_1, hv)}{PDD(z, A_2, f_2, hv)} = \left(\frac{BSF(A_2, hv)}{BSF(A_1, hv)}\right) \times \left(\frac{\left(\frac{f_1 + z_{max}}{f_1 + z}\right)}{\left(\frac{f_2 + z_{max}}{f_2 + z}\right)}\right)^2 \qquad (2\text{-}13)$$

For similar field sizes, the ratio of *BSF* can be assumed to equal 1.

b) Tissue Air Ratio (*TAR*)

Tissue Air Ratio (*TAR*) is the ratio of the doses at point *Q* in the animal body or phantom, D_Q, to the same point *Q* in air surrounded by small mass of tissue, D'_Q, under the same field size at the point *Q*, A_Q, and distance from the source. Refer to Figure 2-7 for the setup of *TAR*.

$$TAR(z,A_Q,\ hv)=\frac{D_Q}{D_Q'} \qquad (2\text{-}14)$$

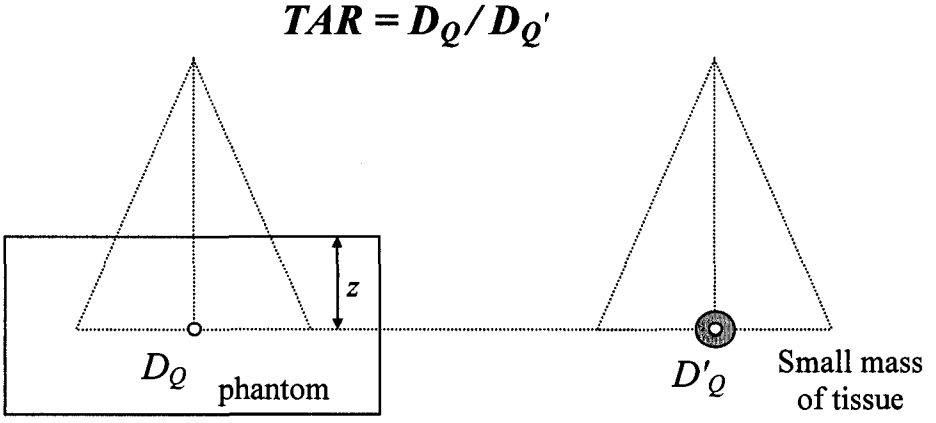

Figure 2-7: Setup for tissue air ratio (TAR) measurements.

Similar to *PDD*, *TAR* increases with increasing beam quality *hv*, decreases with increasing depth *z* and increases with field size A_Q for the same reasons mentioned for *PDD*. However, *TAR* does not depend on the source to surface (or axis) distance *f* for distances between about 50 to 150 cm.[1]

Notice that peak scatter factor is a special case of *TAR* where the doses are at point *P* at depth of maximum dose. i.e., $D_Q = D_P$ (where $z = z_{max} = 0$ cm)

c) Tissue Phantom Ratio (*TPR*) and Tissue Maximum Ratio (*TMR*)

Tissue Phantom Ratio (*TPR*), as shown in Figure 2-8, is the ratio of the doses at point *Q* with depth *z* in the animal body or phantom, to a reference point Q_{ref} at depth z_{ref}, under the same field size A_Q, and with a fixed source to point of measurement distance:

$$TPR(z,A,\ hv)=\frac{D_Q}{D_{Q_{ref}}} \qquad (2\text{-}15)$$

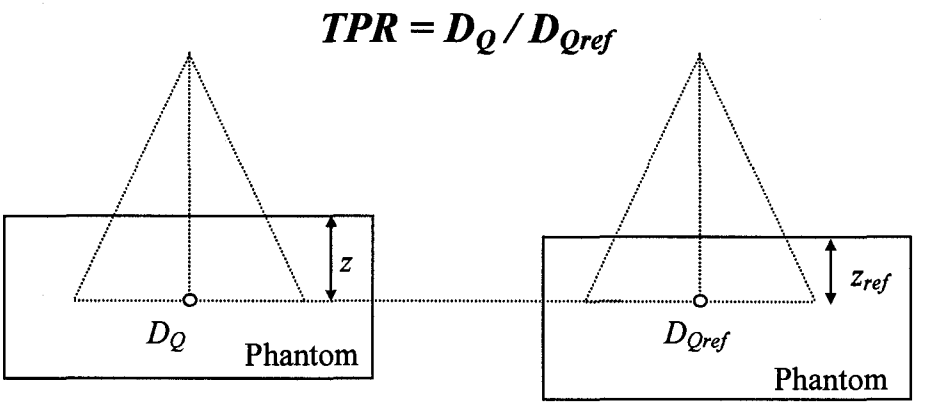

Figure 2-8: Setup for tissue phantom ratio (TPR) measurements.

If the reference point Q is chosen to be at the point of maximum dose with depth z_{max}, then *TPR* is called Tissue Maximum Ratio (*TMR*):

$$TMR(z,A,\ hv)=\frac{D_Q}{D_P} \qquad (2\text{-}16)$$

TPR and *TMR* are similar to *TAR* in their dependence on beam quality *hv*, depth *z* and field size A_Q, and in their independence of the source to surface (or axis) distance *f* for distances between about 50 to 150 cm.[1]

2.10 References

1 E. B. Podgorsak (Editor), *Radiation Oncology Physics : A Handbook for Teachers and Students*. (International Atomic Energy Agency, Vienna, 2005).

2 J. E. Turner, *Atoms, Radiation, and Radiation Protection*, 2nd ed. (J. Wiley, New York, 1995).

3 J. H. Hubbell and S. M. Seltzer, Tables of X-Ray Mass Attenuation Coefficients and Mass Energy-Absorption Coefficients from 1 keV to 20 MeV for Elements Z = 1 to 92 and 48 Additional Substances of Dosimetric Interest NISTIR 5632, National Institute of Standards and Technology (NIST).

4 F. M. Khan, *The Physics of Radiation Therapy*, 3rd ed. (Lippincott Williams & Wilkins, Philadelphia ; London, 2003).

5 H. E. Johns and J. R. Cunningham, *The Physics of Radiology*, 4th ed. (Thomas, Springfield, Ill., 1983).

6 ICRU (International Commission for Radiation Units and Measurements), *Fundamental Quantities and Units for Ionizing Radiation, ICRU Report No. 60.* (1998).

7 "Central axis depth dose data for use in radiotherapy, BJR Supplement no. 25", Br. J. Radiol, (1996).

8 C. M. Ma, C. W. Coffey, L. A. DeWerd et al., "AAPM protocol for 40-300 kV x-ray beam dosimetry in radiotherapy and radiobiology", Med Phys **28** (6), 868-893 (2001).

CHAPTER 3

REFERENCE DOSIMETRY OF LOW ENERGY X-RAY BEAMS

This chapter presents a review of ionization chambers basics. The chapter also discusses the TG-61 protocol for reference dosimetry of kilovoltage X-ray beams.

3.1 Ionization Chamber Basics

An ionization chamber is a device used for the detection or measurement of ionizing radiation and the determination of radiation dose. Two types of ionization chambers are commonly used in beam calibration and radiation dose measurements: cylindrical (thimble) chambers; and parallel-plate (end window or plane-parallel) chambers. Cylindrical chambers are typically used in calibration of orthovoltage (100 – 300 kV) X-ray beams while parallel-plate chambers are often used for the calibration of superficial (< 100 kV) X-ray beams.[1]

3.1.1 Design

An example of a parallel plate ionization chamber is shown in Figure 3-1. It consists of a gas-filled (usually air) cavity between two conductive electrodes: a polarizing electrode, which is connected to the power supply directly, and a measuring electrode, which is connected to ground through the electrometer to measure the charge or current produced in the gas cavity. The two electrodes are separated with a high quality insulator to reduce the leakage current when a polarization voltage is applied to the chamber. A third electrode called the guard electrode further reduces chamber leakage

radiation by intercepting the leakage current and allows it to flow to ground. It also improves the electric field uniformity and defines the ion collecting volume.[1,2]

3.1.2 Exposure Measurement

Ionization chamber based dosimetry systems consist mainly of three components: an ionization chamber; an electrometer; and a power supply. This is shown schematically in Figure 3-1. The circuitry resembles a capacitor (ionization chamber) connected to a battery (power supply), with the electrometer measuring the charge or current induced in the chamber. The power supply is either a stand-alone unit or forms an integral part of the electrometer. It is important that one can change the magnitude and polarity of the voltage supplied, so that the ion collection efficiency of the chamber may be determined.

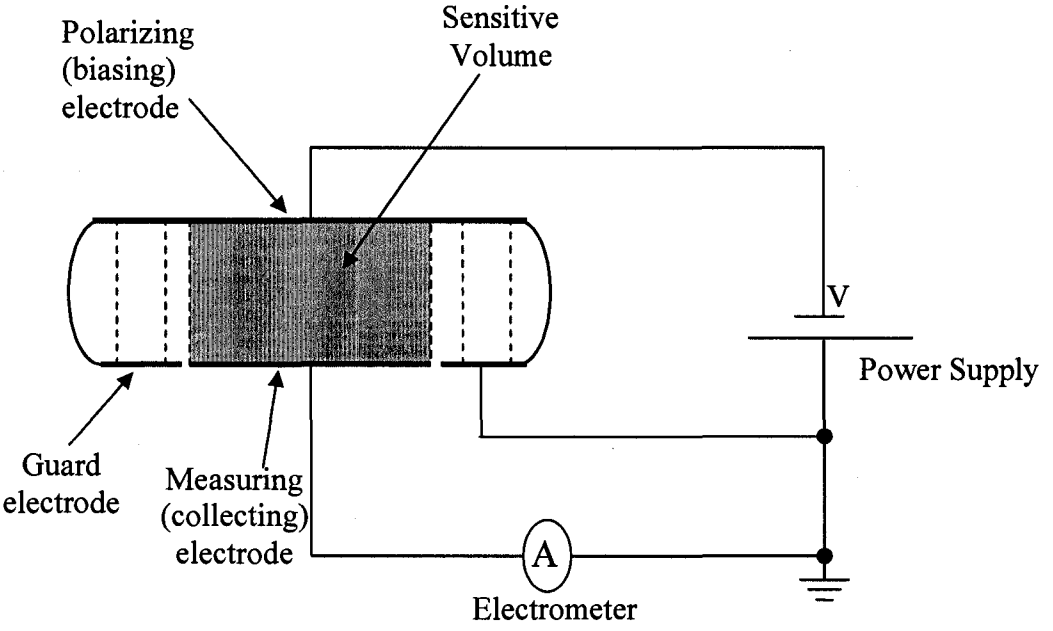

Figure 3-1: A schematic drawing of an ionization chamber based dosimetry system circuitry.[1]

As the low energy X-ray beam interacts with the chamber, it releases electrons in the chamber wall, air cavity, and to less extent in the phantom by photoelectric and

Compton interactions. Some of the resulting electrons produce ionization of air molecules along their tracks inside the chamber sensitive volume. The ionization results in positive ions and low energy electrons which attach themselves to electro-negative oxygen molecules in air forming negative ions. The electric field produced by the voltage applied across the ion-collection plates results in positive ions moving towards the negative electrode and negative ions moving toward the positive electrode. Either sign can be measured by an electrometer.

As mentioned previously in Section 2.8.1, the dosimetric quantity exposure (X) is equal to $\frac{dQ}{dm_{air}}$, where dQ is the sum of all charges of one sign produced as photons travel in a mass dm of air free-in-air. Ionization chambers are calibrated against a standard instrument for radiation qualities of interest. In case of low energy X-rays, the chamber is calibrated against a free-air chamber in National Primary Standard Laboratories.[2] The standards laboratory provides the user with an exposure calibration coefficient N_X where:

$$X = N_X Q \qquad (3\text{-}1)$$

where X is the exposure, Q is the corrected charge reading, and N_X is the exposure calibration coefficient typically given in units of R/nC.

3.1.3 Conversion to Dose in Air

In the kilovoltage range, it is possible to equate the absorbed dose to the collisional kerma (K_{col}) because electrons produced by the X-ray beam have short ranges and thus deposit all their energy locally. The fact that the radiative losses in this energy range and in low atomic number materials can be ignored makes it further possible to

equate the absorbed dose to kerma in air. One can convert the exposure reading X to dose to air using the relation:

$$D_{air} \approx (K_{col})_{air} = X\left(\frac{W_{air}}{e}\right) \qquad (3\text{-}2)$$

where $\left(\frac{W_{air}}{e}\right)$ is the average energy required to produce an ion pair in air. The current value for $\left(\frac{W_{air}}{e}\right)$ is 33.97 eV/ion pair or 33.97 J/C.[3] Using 1 R = 2.58×10^{-4} C/kg, we get Equation 2-8, i.e., $(K_{col})_{air} = X\left(2.58\times10^{-4}\frac{C}{kg}\times 33.97\frac{J}{C}\right) = \left(0.876\frac{cGy}{R}\right)X$.

It is also possible to calibrate the chamber in standard laboratories that provide an air kerma in air calibration coefficient $N_{K,air}$ satisfying the equation:

$$K_{air} = N_{K,air}Q \qquad (3\text{-}3)$$

where K_{air} is kerma to air, Q is the corrected charge reading, and $N_{K,air}$ is the air kerma in air calibration coefficient typically given in unit of cGy/nC. Notice that $D_{air} = K_{air}$ in kilovoltage X-ray beams.[1,2,4]

3.1.4 Signal Correction for Influence Quantities

The chamber calibration is usually performed at a national standards laboratory under certain "reference" conditions. If the chamber is used under different conditions, then the measured signal must be corrected for the influence quantities that are not the subject of the measurement but affect the signal being measured. The major influence quantities are:

(1) Ambient air temperature and pressure: The mass of air in the sensitive volume of the chamber is equal to its density ρ_{air} multiplied by its effective volume V_{eff}. The air

density ρ_{air} is influenced by the atmospheric temperature and pressure since most air chambers are open to the ambient atmosphere. Standard laboratories calibrate the chambers at a reference temperature T_0 (22 ^{0}C in North America, 20 ^{0}C in most other places[2]) and a reference pressure P_0 (101.325 kPa). The user multiplies the chamber reading by a temperature-pressure correction factor $k_{T,P}$ given as:

$$k_{T,P} = \frac{(273.2+T)}{(273.2+T_0)}\frac{P_0}{P} \qquad (3\text{-}4)$$

Where P and T (^{0}C) are chamber air pressure and temperature, respectively, at the time of measurement, while P_0 and T_0 are the reference condition used in the standard laboratory.

(2) Chamber polarity effects: Applying an opposite polarizing potential to the ionization chamber may yield different readings under identical irradiation conditions. This is known as the polarity effect. The polarity effect depends on beam quality and cable arrangement and should be measured and corrected for. The true reading is taken to be the mean of the absolute values of readings taken at the two polarities. Thus the polarity correction factor k_{pol} is given by:

$$k_{pol} = \frac{|M_+| + |M_-|}{2M} \qquad (3\text{-}5)$$

where M_+ is the reading when positive charge is collected, M_- is the reading when negative charge is collected, and M (one of M_+ and M_-) is the reading obtained at the polarity used routinely. In both cases, the sign of M must be used and usually M_+ and M_- have opposite signs unless the background is large.[1,4]

(3) Chamber voltage effects: The response of an ionization chamber depends, among other factors, on the voltage applied between the measuring and polarizing electrodes of the chamber. The complete collection of the ions formed by the radiation is

required to determine accurately the dose absorbed in the air in the ionization chamber cavity. Some of the ions recombine with ions of the opposite charge on their way to the collection electrode and are not collected. One can estimate the true number of ions formed from measurements made with two different voltages. This is done usually by using the normal collecting voltage and half that voltage. For continuous beams, the two-voltage approach yields an ion recombination correction factor k_{ion} given as:[5]

$$k_{ion} = \frac{1 - \left(\frac{V_H}{V_L}\right)^2}{\frac{M_H}{M_L} - \left(\frac{V_H}{V_L}\right)^2} \qquad (3\text{-}6)$$

where V_H is the normal collecting voltage for the detector, M_H is the chamber reading with bias V_H, and M_L is the raw chamber reading at bias V_L, where $V_L / V_H < 0.5$.[4]

(4) Chamber leakage currents: No matter how well an ionization chamber dosimetric system is designed, there will always be a small signal when the system is on and there is no radiation. This leakage signal is not related to radiation and is called intrinsic (dark) current. It results from surface and volume leakage currents flowing between the polarizing and measuring electrodes of the ionization chamber. The intrinsic leakage currents should be at least two orders of magnitude lower than the measured radiation induced signals, and are thus either negligible or can be corrected for by performing a leakage current measurement. Following the irradiation of insulators and chamber parts; cables and electronics of the measuring equipment, electric leakage in the ionization chamber and electrometer may also occur. This is referred to as post-irradiation leakage, an effect that continues after the irradiation and usually decreases exponentially

with time. Leakage current also can be caused from mechanical stress on cable insulators.[1]

(5) Chamber stem effects: Irradiation of the chamber stem results in a different type of current not related to the true radiation, and this is referred to as the stem effect. The two main mechanisms are stem scatter, which is caused by scattered radiation in the stem reaching the chamber volume; and stem leakage, which is caused by direct irradiation of the chamber volume as well as the insulators and cables in the chamber. The stem scatter can be corrected with a stem factor P_{stem}, if the chamber is to be used under a different field size than the field size at which it was calibrated, by comparing the chamber with unknown P_{stem} with a reference chamber for which P_{stem} is known.[4] The stem leakage, on the other hand, is included in the polarity correction.[1]

3.2 TG-61 Procedures for Kilovoltage Dosimetry

TG-61[4] is a protocol for 40–300 kV X-ray beam dosimetry used in radiotherapy and radiobiology published by the American Association of Physicists in Medicine (AAPM). The protocol is based on ionization chambers calibrated in air in terms of air kerma. The protocol presents two methods for calibration: The ''In-Air method'' which is a calibration method to obtain absorbed dose to water at the surface of a water phantom, based on an in-air measurement using an ion chamber calibrated in free air; and ''In-Phantom method'' which is a calibration method to obtain absorbed dose to water at 2 cm depth in water, based on an in-water measurement using an ion chamber calibrated free in air.

A. The "In-Air method": This method can be used for low and medium energy X-rays (between 40 kV and 300 kV tube potential). The method determines the absorbed dose to water at the surface (i.e., the reference depth $z_{ref} = 0$). The equation for absorbed dose to water at the phantom surface is:

$$D_{air,z=0} = M N_K B_w P_{stem,air} \left[\left(\frac{\mu_{en}}{\rho} \right)_{air}^{W} \right]_{air} \qquad (3\text{-}7)$$

where M is the free-in-air chamber reading, corrected for temperature, pressure, ion recombination and polarity effects, with the center of the sensitive air cavity of the ionization chamber placed at the measurement point ($z_{ref} = 0$); N_K is the air kerma calibration coefficient for the given beam's quality; B_w is the backscatter factor which accounts for the effect of the phantom scatter; $P_{stem,air}$ is the chamber stem correction factor accounting for the change in photon scatter from the chamber stem between the calibration and measurement, mainly due to the change in field size, it is taken as unity if the same field size is used in the calibration and the measurement; $\left[\left(\bar{\mu}_{en} / \rho \right)_{air}^{W} \right]_{air}$ is the ratio for water-to-air of the mean mass energy-absorption coefficients averaged over the incident photon spectrum free in air. The values of B_w and $\left[\left(\bar{\mu}_{en} / \rho \right)_{air}^{W} \right]_{air}$ tabulated in the TG-61 protocol were determined experimentally and verified by Monte-Carlo simulation.[6,7,8,9] Equation (3-7) gives the absorbed dose assuming dose and kerma equivalence and in the absence of electron contamination from the primary beam.

B. The "In-Phantom method": This method is recommended for medium-energy X-rays (between 100 kV and 300 kV tube potential) only. It determines the absorbed dose to water at 2 cm depth in water. The protocol adopted a reference depth of 2 cm in water because for smaller depths there may be not enough buildup material in the upstream

direction to cover the whole chamber; for depths larger than 2 cm the chamber signal may be too small. The absorbed dose to water at the 2 cm reference depth (z_{ref}= 2 cm) in water for a 10×10 cm^2 field defined at 100 cm SSD can be determined using the following equation:

$$D_{w,z=2} = MN_K P_{Q,cham} P_{sheath} \left[\left(\frac{\bar{\mu}_{en}}{\rho} \right)^{w}_{air} \right]_{water} \qquad (3\text{-}8)$$

where M is the chamber reading, corrected for temperature, pressure, ion recombination, and polarity effects, with the center of the air cavity of the chamber placed at the reference depth; N_K is the air kerma calibration coefficient for the given beam's quality; $P_{Q,cham}$ is the overall chamber correction factor that accounts for the change in the chamber response due to the displacement of water by the ionization chamber (air cavity plus wall) and the presence of the chamber stem, the change in the energy, and angular distribution of the photon beam in the phantom compared to that used for the calibration in air; P_{sheath} is the correction for photon absorption and scattering in the waterproofing sleeve, if present; and $\left[(\bar{\mu}_{en} / \rho)^{w}_{air} \right]_{water}$ is the ratio for water-to-air of the mean mass energy-absorption coefficients, averaged over the photon spectrum at the reference point in water in the absence of the chamber. The values for $\left[(\bar{\mu}_{en} / \rho)^{w}_{air} \right]_{water}$, P_{sheath} *and* $P_{Q,cham}$ provided in the TG-61 protocol are taken from different references.[7,10,11,12,13,14,15]

3.3 References

[1] E. B. Podgorsak (Editor), *Radiation Oncology Physics : A Handbook for Teachers and Students*. (International Atomic Energy Agency, Vienna, 2005).

[2] F. M. Khan, *The Physics of Radiation Therapy*, 3rd ed. (Lippincott Williams & Wilkins, Philadelphia ; London, 2003).

[3] M. Boutillon and A. M. Perroche-Roux, "Re-evaluation of the W value for electrons in dry air", Phys Med Biol **32**, 213-219 (1987).

[4] C. M. Ma, C. W. Coffey, L. A. DeWerd et al., "AAPM protocol for 40-300 kV x-ray beam dosimetry in radiotherapy and radiobiology", Med Phys **28** (6), 868-893 (2001).

[5] M. S. Weinhous and J. A. Meli, "Determining P_{ion}, the correction factor for recombination losses in an ionization chamber", Med Phys **11** (6), 846-849 (1984).

[6] S. C. Klevenhagen, R. J. Aukett, R. M. Harrison et al., "The IPEMB code of practice for the determination of absorbed dose for x-rays below 300 kV generating potential (0.035 mm Al-4 mm Cu HVL; 10-300 kV generating potential)", Phys Med Biol **41** (12), 2605-2625 (1996).

[7] S. C. Klevenhagen, "Experimentally determined backscatter factors for x-rays generated at voltages between 16 and 140 kV", Phys Med Biol **34**, 1871-1882 (1989).

[8] R. T. Knight and A. E. Nahum,"Depth and field-size dependence of ratios of mass-energy-absorption coefficient, water-to-air, for kV X-ray dosimetry", *in*

Proceedings of the of the IAEA International Symposium on Measurement Assurance in Dosimetry,(IAEA, Vienna, 1994)

[9] C. M. Ma and J. P. Seuntjens, "Mass-energy absorption coefficient and backscatter factor ratios for kilovoltage x-ray beams", Phys Med Biol **44** (1), 131-143 (1999).

[10] C. M. Ma and J. P. Seuntjens, "Correction factors for water-proofing sleeves in kilovoltage x-ray beams", Med Phys **24** (9), 1507-1513 (1997).

[11] C. M. Ma and A. E. Nahum, "Monte Carlo calculated stem effect correction for NE2561 and NE2571 chambers in medium-energy x-ray beams", Phys Med Biol **40** (1), 63-72 (1995).

[12] C. M. Ma and A. E. Nahum, "Calculations of ion chamber displacement effect corrections for medium-energy x-ray dosimetry", Phys Med Biol **40** (1), 45-62 (1995).

[13] C. M. Ma and A. E. Nahum,"Monte Carlo calculated correction factors for a NE2571 chamber in medium-energy photon beams", *in Proceedings of the IAEA International Symposium on Measurement Assurance in Dosimetry*, edited (IAEA, Vienna, 1994)

[14] J. Seuntjens and F. Verhaegen, "Dependence of overall correction factor of a cylindrical ionization chamber on field size and depth in medium-energy x-ray beams", Med Phys **23** (10), 1789-1796 (1996).

[15] J. Seuntjens, H. Thierens, and U. Schneider, "Correction factors for a cylindrical chamber used in medium-energy x-ray beams", Phys. Med. Biol. **38**, 805-832 (1993).

CHAPTER 4

MATERIALS AND METHODS

This chapter gives a description of the Faxitron model CP160 X-ray irradiator located at the Montreal General Hospital and also discusses the materials and the experimental techniques used in this project.

4.1 Faxitron Model CP160 X-Ray Irradiator Description

The Faxitron (Faxitron X-ray Corporation, Wheeling, IL) is a low-energy X-ray irradiator used for research studies such as specimen irradiation, cancer oncology research, small animal irradiation, animal food irradiation, laboratory scale sterilization studies and plant and seed irradiation.

The X-ray unit is housed in a shielded cabinet. Specimens are irradiated on a rotating turntable (speed of rotation = 2 RPM) or stationary shelf at different positions; from a source to shelf distance (SSD) of 12.7 cm at the first shelf to 99 cm at the floor of the cabinet. The field size changes with these SSDs from 10.3 cm diameter at the first shelf to cover the whole shelf (about 72 cm diameter) at the floor of the unit. Table 4-1 lists the SSD, and field size of each shelf position.

Shelf #	SSD (cm)	Diameter (cm)
9	12.7	10.3
8	22.9	18.5
7	33	26.7
6	43.2	34.9
5	53.4	43.1
4	63.5	51.3
3	73.7	59.5
2	83.8	72
1	94	72
Floor	99.1	72

Table 4-1: Source to surface of tray distance and field size at each shelf position. At shelves # 3, 2 and 1, the radiation field covers the entire tray.

. The machine is able to produce X-ray beams of energies ranging from 10 to 160 kVp, with tube current ranging from 100 μA to 10 mA. Time of exposure can be set from 0.1 to 99.9 minutes in steps of 0.1 minute. The X-ray tube has a stationary anode (target) made of tungsten. Two focal spot sizes can be set: large with 5.5 mm diameter, and small with 1 mm diameter. The large focal spot is used typically for irradiation, while the small one is used for imaging as it gives a better spatial resolution. The tube has a beryllium window, 0.8 mm thick, as inherent filtration. Added filtration of 0.5 mm thick Aluminum, 0.5 mm thick Copper (both came with the machine), or any custom thickness/material can be placed beyond the exit window to yield different beam qualities.

The output for the machine, as quoted by the manufacturer,[1] for a beam energy of 160 kVp, current setting of 6.3 mA and source-shelf distance of 33 cm is 1450 R/min for a non-filtered beam, 265 R/min for a 0.5 mm Al filtered beam, and 73 R/min for a 0.5 mm Cu filtered beam.

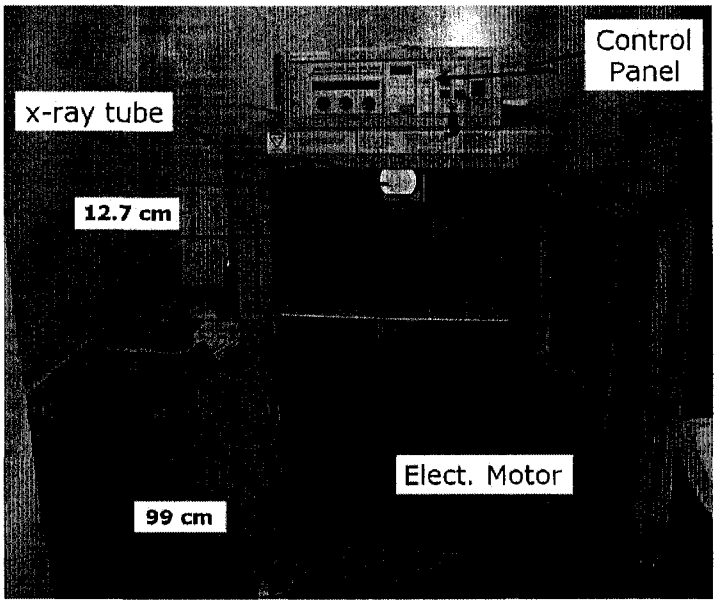

Figure 4-1: The Faxitron model CP160 X-ray irradiator.

4.2 Measuring Instruments

4.2.1 Ion Chambers and Electrometers

The main ion chamber used for beam characterization and calibration, film calibration and half-value layer measurements was a cylindrical (Farmer-type) ionization chamber model NE2571 (Nuclear Enterprises, Fairfield, NJ). It has a sensitive volume of approximately 0.6 cc.[2] The chamber was chosen mainly because of its robust nature and its relatively high signal to noise ratio. A custom build-up cap made of Solid Water was available to be used with this chamber for in-phantom measurements. NE2571 chamber was used with Keithley 35617 (Keithley Instruments Inc., Cleveland, OH) digital electrometer which can supply voltages between -1000 V and +1000 V to the chamber.

A Wellhöfer PPC40 (Scanditronix Wellhöfer North America, Berlet, TN) parallel plate (Roos-type) chamber was used for the relative dose measurements in water because

of its water-proof properties. The PPC40 has a collecting volume of 0.4 cc.[3] The chamber was used with a Keithley 6517A digital electrometer.

The radiation level around the Faxitron CP160 unit was surveyed using a Victoreen 190 (Victoreen Instrument Co., Cleveland, OH) survey meter with its gamma GM probe. The survey meter features autodose accumulation and measures within an operating range of 1 mR/hr to 1 R/hr or 1 to 1,000,000 cpm.

4.2.2 Films

The two major types of current film dosimeters are radiographic film and radiochromic film. Radiographic film is made of a base of thin plastic with a radiation sensitive emulsion (silver bromide (AgBr) grains suspended in gelatine) coated uniformly on one or both sides of the base. Radiographic film exhibits large differences in sensitivity for different energies between 10 keV and 200 keV, and is not tissue equivalent. Moreover, it is sensitive to room light, and requires chemical processing after irradiation.[4]

The newer type of film, radiochromic film, contains a special dye that is polymerized upon exposure to radiation. Radiochromic film is colourless with a nearly tissue equivalent composition. This type of film is self-developing, and in general, it does not exhibit severe dependence on energy compared to radiographic film.[5]

In this work, Kodak EDR2 radiographic films (Kodak, Rochester, NY) were used for radiation field-tray marking correspondence measurements only, while Gafchromic EBT films (Nuclear Associates, Hicksville, NY) were used for profile measurements and verification of the dose delivered.

The Gafchromic EBT film was calibrated using a published protocol[6] for the 160 kVp 0.5 mm Cu filtered beam. The films were digitized with an Agfa Arcus II desktop flat-bed scanner and its FotoLook 3.5 software in the 48-bit RGB transmission mode, with the maximum OD range and all filters and image enhancement options turned off. The scanned images were imported into an image manipulation routine written with MatLab 7.0 (Math Works, Natick, MA) that extracts the red component of the RGB scanned image, applies a 2D zero-phase Wiener filter, and subsequently determines the net optical density. The resulting optical density values were fitted to a 5^{th} order polynomial to obtain the final calibration curve using the TableCurve 2D v5.1.1 software (SYSTAT Software Inc., Richmond, CA).

4.3 Trays, Jigs, and Phantoms

The Faxitron CP160 unit comes with its own tray made of plastic, about 0.4 cm thick. The manufacturer tray is shown in Figure 4-2 (a). An electrical motor, attached underneath the tray, controls the rotation of a removable plastic turntable that can be mounted on top of the tray.

Two more trays, about 0.4 cm thick, were made out of Plexiglas for the measurements of half-value layer. The first one, shown in Figure 4-2 (b), was covered with a thin sheet (2 mm) of lead to attenuate scattered photons. A hole with diameter of 11 cm centered at the beam central axis was made. A 15x15 cm^2, 0.4 cm thick lead collimator with a 1.2 cm diameter hole in the center was used to collimate the beam when put on top of this tray. The second tray, shown in Figure 4-2 (c), was used to hold the

aluminium or copper sheets (attenuators) and it has a hole with diameter of 6 cm centered at the beam central axis.

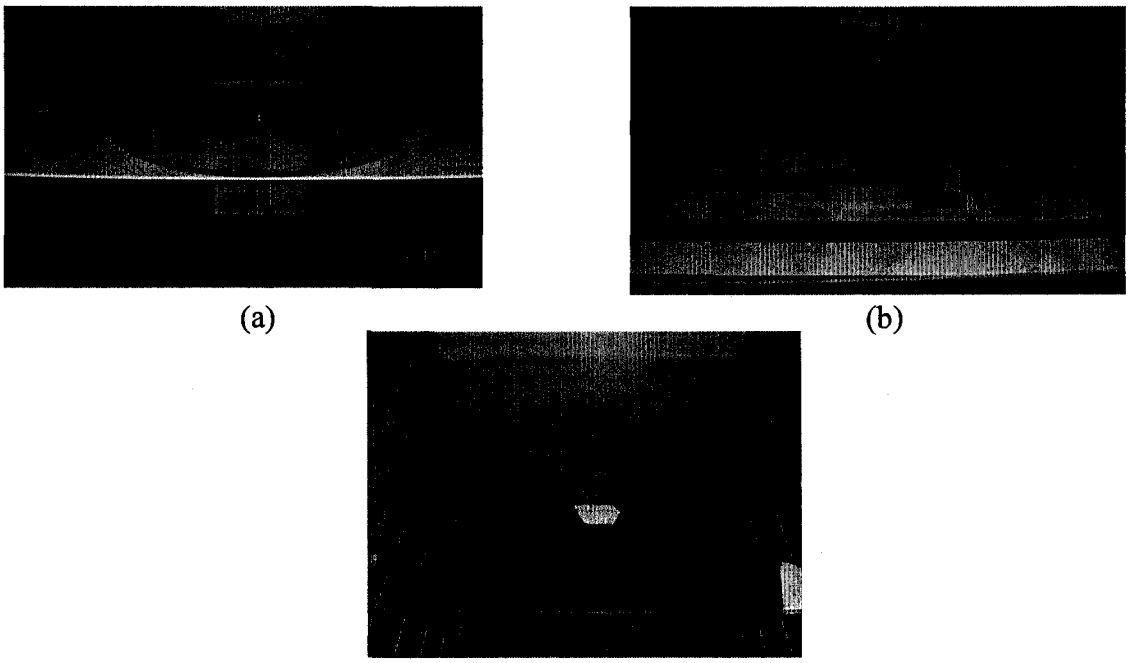

(a) (b)

(c)

Figure 4-2: Three different trays used with Faxitron CP160: (a) Manufacturer tray with its plastic turntable, (b) Lead-covered tray, and (c) Plastic tray for holding attenuators.

A special jig, shown in Figure 4-3, was used for the Gafchromic EBT film measurements in air. The jig consists basically of two wires hung in air between two Plexiglas holders that are based on a large piece of Plexiglas. The distance between the wires and the base is about 30 cm.

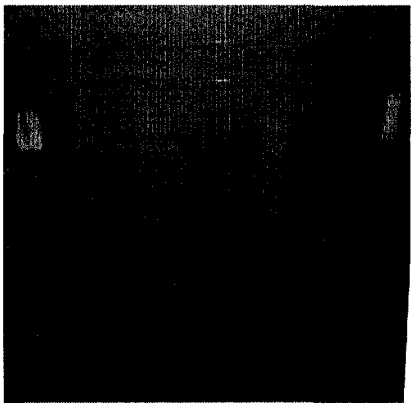

Figure 4-3: A special jig used for the in air film measurements.

A special mouse phantom (length 7 cm, width 3 cm, height 3 cm) was made out of Solid Water for the mouse irradiation experiments. The mouse phantom has a hole in it allowing the NE2571 chamber with its build-up cap to fit in and set it at the center of the phantom.

Scattering material made of polymethyl methacrylate (PMMA), 3 cm thick, were arranged around the mouse phantom in such a way to make a 10×10 cm^2 large phantom, as shown in Figure 4-4, to increase the dose output delivered to the mouse phantom and thus reduce time of irradiation.

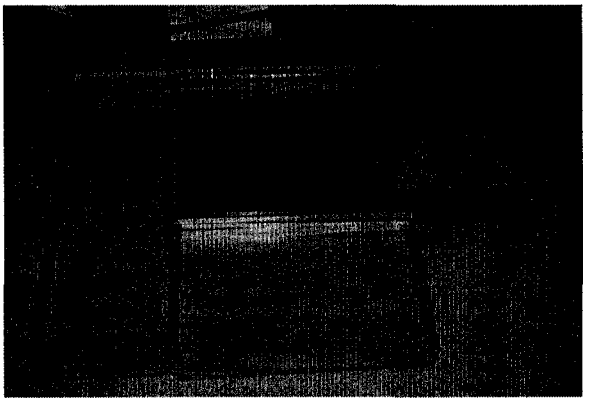

Figure 4-4: A 10×10 cm^2 large phantom with NE2571 chamber inside. The mouse phantom made of Solid Water is shown in the center surrounded by PMMA scattering materials.

4.4 Characterization Experiments

4.4.1 Radiation Survey

The radiation survey around the irradiator was carried out using the Victoreen 190 survey meter with its gamma GM probe while the machine was operated at its maximum output, i.e., at 160 kVp and 6.3 mA.

4.4.2 Radiation Field-Tray Marking Correspondence

A Kodak EDR2 radiographic film was put on the company tray and pin holes were made to mark the center of the field as indicated by the tray's marks. Mutli-irradiations were made for this film where the tray was moved from one shelf position to another to check the tilting of the X-ray tube.

4.4.3 Beam Profile

Profile measurements were done using Gafchromic EBT films at shelf #9 (SSD = 12.7 cm) for the 160 kVp 0.5 mm Cu filtered beam. The films were put on top of the company tray with the turntable off. Another profile measurement to investigate the usefulness of rotation was done while the turntable was on doing full rotations. Also, a profile measurement at the center of a 3 cm thick Solid Water phantom was taken.

4.4.4 Half-Value Layers and Effective Energies

The attenuation curve measurements in copper were done for 100, 120, 140, and 160 kVp for the 0.5 mm Cu filtered beams, and in aluminium for the 60 and 80 kVp beams. For both the 0.5 mm Al filtered and the non-filtered beams, the measurements in aluminium were done for 20 up to 160 kVp in steps of 20 kVp.

For all HVL measurement experiments, the Lead-covered tray was placed at shelf position #9 (SSD = 12.7 cm) with the 1.2 cm diameter hole lead collimator on it. The plastic tray was put at shelf position #8 (SSD = 22.9 cm), i.e., 10 cm away from the collimator, with attenuators (copper or aluminium) of varying thickness on it. The NE2571 chamber was placed at a source-chamber distance (SCD) of 63.5 cm. The 1.2 cm diameter hole lead collimator at shelf position #9 yields a small field size of 6 cm diameter at the position of the chamber, 50 cm away from the collimator. The position of the chamber at the center of the beam was verified using films. Figure 4-5 shows the setup of HVL measurements.

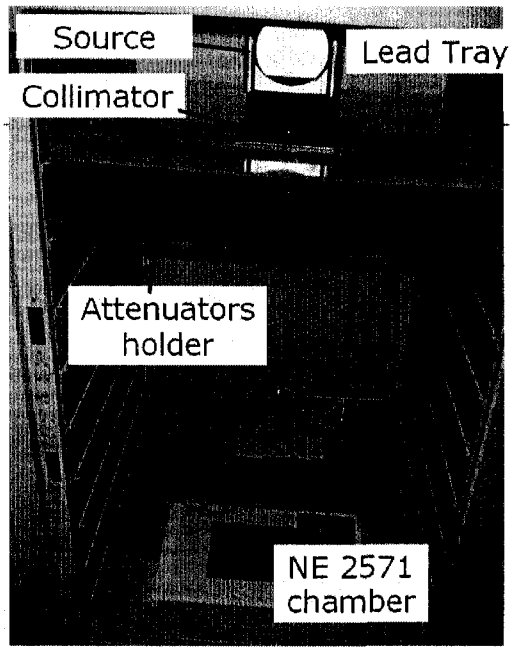

Figure 4-5: Setup for HVL measurement

Mass attenuation coefficients were calculated from the HVLs using the relationship (see Equation 2-5):

$$\frac{\mu}{\rho} = \frac{1}{\rho} \frac{\ln(2)}{HVL} \qquad (4\text{-}1)$$

where ρ is the density of the attenuator. The effective energy was determined using NIST database[7] which tabulates the mass attenuation coefficients as a function of energy.

4.4.5 Chamber Calibration

The NE2571 chamber, used with the Keithley 35617 electrometer, was cross-calibrated with orthovoltage and superficial units located at the Sir Mortimer B. Davis - Jewish General Hospital (JGH) with a similar chamber (NE2505) for energies ranging between 50 kVp and 250 kVp (HVL 0.25 mm Al – 2 mm Cu). The cross-calibration was done in air with no build-up cap or scattering materials. Two curves for air kerma calibration coefficient N_K and exposure calibration coefficient N_X were obtained from the cross-calibration. The calibration of the JGH's NE2505 chamber was carried out by the National Research Council of Canada (NRC) standards laboratory.

4.4.6 Measured Outputs

The outputs in air at shelf position #7 (SCD = 33 cm) and current setting of 6 mA were measured for energies ranging between 60 and 160 kVp for the Cu filtered beam, and between 20 and 160 kVp for both the 0.5 mm Al filtered and the non-filtered beam in steps of 10 kVp. The output, in terms of water dose rate in air (cGy/min), is calculated using the formula:

$$\left(\dot{D}_W\right)_{air} = \dot{M} N_K \left[\left(\frac{\mu_{en}}{\rho}\right)^W_{air}\right]_{air} \qquad (4\text{-}2)$$

while the output, in terms of exposure rate (R/min), is calculated using the formula:

$$\dot{X} = \dot{M} N_X \qquad (4\text{-}3)$$

where $\dot{M}$ is the chamber charge reading for one minute in air corrected for temperature and pressure; N_K is the air kerma calibration coefficient for the energy being used; N_X is the exposure calibration coefficient for the energy being used; and $\left[\left(\frac{\mu_{en}}{\rho}\right)^{W}_{air}\right]_{air}$ is the ratio of water-to-air mean mass energy-absorption coefficients averaged over the incident photon spectrum free in air for the radiation quality used.

4.4.7 Output Constancy

Three tests were carried out to check the output constancy: reproducibility test, long term constancy test and constancy during prolonged exposure.

a) Output Reproducibility: The NE2571 chamber was placed at SCD = 36.8 cm and exposed for 1 minute with the 160 kVp non-filtered beam and current setting of 6.3 mA, the measurement was repeated twenty times. The same experiment was performed for the 100 kVp non-filtered beam and current setting of 10 mA with SCD = 44.5 cm.

b) Long Term Constancy: Seven readings were taken over 46 days. The PPC40 chamber was placed each time on the center of the tray at shelf #7 (SCD = 32 cm) and exposed for 1 minute with the 160 kVp 0.5 mm Cu filtered beam and current setting of 6 mA.

c) Constancy during Prolonged Exposure: The NE2571 chamber was placed at SCD = 32 cm in air and exposed for 30 minutes with the 160 kVp non-filtered beam and current setting of 6.3 mA. Readings of current were recorded every 12 seconds.

4.4.8 Absolute Output vs. kVp

The data obtained from the measured outputs experiment described in Section 4.4.6 were used to investigate the output vs. kVp relationship.

4.4.9 Relationship between Output, mA and Time

For the output vs. mA experiment, the NE2571 chamber was placed in air and irradiated with the 100 kVp beam of various current settings starting at 0.5 mA up to 10 mA. The experiment was performed for each of the three qualities: non-filtered beam, 0.5 mm Al filtered beam, and 0.5 mm Cu filtered beam. The same experiment was performed with the 160 kVp energy for the three beam qualities as well, and for current settings starting at 0.5 mA up to 6.3 mA.

The output vs. time experiment was done for the 0.5 mm Cu filtered beam, with irradiation technique of 160 kVp and 6 mA. The NE2571 chamber was placed in air at SCD = 33 cm and readings were taken for irradiation time varying between 0.1 and 20 minutes.

4.4.10 Output Reciprocity with mAs

The control panel does not allow for settings of mAs. However, one can choose different combinations of current (mA) and time settings to produce the required mAs setting. This should, in theory, produce the same output regardless of the combination used. The experiments were done for different combinations of time and mA shown in Table 4-2 using the NE2571 chamber placed in air at SCD = 25 cm.

Beam Quality	mAs	mA	Time (min)
160kVp + 0.5 mm Cu Filter	1800	3	10
		5	6
		6	5
100 kVp + 0.5 mm Cu Filter	600	1	10
		2	5
		4	2.5
		5	2
		10	1
	1200	2	10
		4	5
		5	4
		10	2
	1800	3	10
		5	6
		10	3
	2400	2	20
		5	8
		10	4

Table 4-2: Different combinations of mA and time to produce a specific mAs for the reciprocity test.

4.4.11 Shutter Error

The shutter error is due to a very short lag in the time when the X-ray tube is turned on to the point that it reaches its full output dose rate. This may be due to a lag in the tube's high voltage power source or in the filaments high current source. A correction time can be determined to compensate for the shutter error using the double exposure method[8], where the chamber is exposed with a long exposure time T and the dose D_1 is recorded, another measurement of D_n is done with n dose segments each having an exposure time T/n that is cumulatively equal to T. The shutter correction time t_s can be calculated using the formula:

$$t_s = \frac{(D_n - D_1)T}{(nD_1 - D_n)} \tag{4-4}$$

The experiment was done for T = 10 minutes, and for T/n = 1 minute with 10 segments under the 160 kVp 0.5 mm Cu filtered beam and current setting of 6 mA. The NE2571 chamber was placed in air at SCD = 33 cm.

4.4.12 Inverse Square Law

The inverse square law validation measurements were performed for the three qualities: non-filtered, 0.5 mm Al filtered, and 0.5 mm Cu filtered 160 kVp beam. The NE2571 chamber was placed in air at the center of the beam and the distance to the focal spot indicated on the tube was verified using a tape measure. Measurements were performed at various shelf positions.

Also, the validity of the inverse square law around shelf position #7 (SCD between 28 cm and 38 cm) was further investigated for the 160 kVp 0.5 mm Cu filtered beam because of its importance for the laboratory irradiations. Measurements with SCDs varying by 1 cm were performed for this configuration.

4.4.13 Tray Factors

The tray factor, as defined in this work, is a measure of the change in dose due to the scatter introduced by the tray itself. Tray factors were measured in air for the company tray with turntable for shelf positions #9, #8 and #7 for the 160 kVp 0.5 mm Cu filtered beam, and for shelf position #7 for the non-filtered and 0.5 mm Al filtered 160 kVp beams using the NE2571 chamber. The tray factor is defined as:

$$TF = \frac{M_{Tray}}{M_{NoTray}} \tag{4-5}$$

where M designates the chamber reading.

4.5 Operational Commissioning

One main objective of this work is to commission the Faxitron CP160 irradiator for cell irradiation and small animal irradiation. The focus was on the 160 kVp 0.5 mm Cu filtered beam since it produces the most penetrating beam. Shelf #7 (SSD = 33 cm) was chosen because of its suitable field size and source to surface distance. Nevertheless, commissioning was done for other beam qualities for cell irradiation since they give higher outputs and there is no need for high penetrative power in this case.

4.5.1 Outputs on Tray for Cell Irradiation Configuration

The output was measured using the NE2571 chamber at top of the tray with its turntable for the four upper shelf positions: #9, #8, #7, and #6 (SSD 12.7, 22.9, 33 and 43.2 cm, respectively). This was performed for both the 160 kVp - 6 mA, and 100 kVp - 10 mA techniques for all the three quality beams: 0.5 mm Cu filtered, 0.5 mm Al filtered and non-filtered. The output in terms of water dose rate in air with units of cGy/min is calculated using Equation 4-2, while the output in terms of exposure rate with units of R/min is calculated using Equation 4-3. Note that in this case, the reading of the chamber ($\dot{M}$) incorporates the backscatter from the tray in it, i.e., this is the In-Air method for absolute dose determination described in the TG-61[9] (Equation 3-7) with the B_w being the tray factor or backscattering from the tray and $P_{stem,air}$ is assumed to be incorporated in the chamber reading.

4.5.2 Irradiation Procedure for Cell Cultures

The dose rate delivered to the small mass of cells inside a tissue culture flask is assumed to be equal to water dose rate in air at the surface of the turntable multiplied by an inverse square factor and a flask factor. i.e.,

$$\left(\dot{D}_W\right)_{air} = O_{Tray} \times ISF \times FF \qquad (4\text{-}6)$$

where O_{Tray} is the output in terms of water dose rate in air on the tray; *ISF* is the inverse square factor to correct for the difference in the output at the base of the culture flask; and *FF* is the flask factor.

The flask factor (*FF*) was measured to investigate the amount of attenuation through the wall of the flask by comparing the NE2571 chamber readings on the tray with and without the flask.

To verify the irradiation procedure in a laboratory mode, Gafchromic EBT film measurements were performed for the 160 kVp 0.5 mm Cu filtered beam with current setting of 6 mA at the upper three shelves (SSD = 11.7, 21.9, and 32 cm respectively). The films were put inside the tissue culture flask on the turntable and the doses delivered to the films were compared to the expected values when using Equation (4-6).

Also, an "experimental" geometry was set to validate our formalism. The tissue culture flask, with a piece of film placed inside, was put on top of a $30\times30\times10$ cm^3 Solid Water phantom, to provide enough backscatter, at SSD = 29 cm. The time required to deliver a target dose of 100 cGy to the cells using 160 kVp 0.5 mm Cu filtered beam and current setting of 6 mA was calculated and the actual dose delivered, as read by the film, was compared with the target dose.

4.5.3 Measurements of Dosimetric Functions: *BSF*, *TMR*, *TAR* and *PDD*

The measurements of backscatter factors (*BSF*) were performed at SSDs = 20.4 , 30.5 and 40.7 cm for the 160 kVp 0.5 mm Cu filtered beam, and at SSD = 30.5 cm for the 160 kVp 0.5 mm Al filtered beam. The PPC40 parallel plate chamber with the Keithley 6517A digital electrometer were used for these measurements. The chamber was put at the SSD under investigation first free in air, and then inside a small water tank of size 30 × 30 × 30 cm^3 at the surface of water, and was irradiated for the same period of time. The backscatter factor is defined as:

$$BSF(A, hv) = \frac{D_{Water\ at\ z_{max}}}{(D_{Water})_{Air}} \qquad (4\text{-}7)$$

where *D* designate the dose as read by the chamber, calculated according to Equation 4-2.

Tissue Maximum Ratio (*TMR*) measurements were done using the small water tank at shelf positions #8, #7, #6 (source-axial distances (SADs) = 20.4 , 30.5 and 40.7 cm, respectively) for the 160 kVp 0.5 mm Cu filtered beam, and at shelf position #7 (SAD = 30.5 cm) for the 160 kVp 0.5 mm Al filtered beam. These SADs are shorter than the source-tray distance of each shelf under investigation by 2.5 cm, corresponding to the theoretical positioning of the center of a 3 cm mouse positioned on top of the turntable (1 cm thick). The tank was first filled up with water to the surface of the PPC40 chamber, then more layers of water were added while keeping the chamber in the same position. The readings were corrected for temperature changes during the filling process.

Tissue Air Ratio (*TAR*) values for a certain field size (*A*) and beam quality (*hv*) are calculated by multiplying *TMR* values by *BSF* of that field size and beam quality:[10]

$$TAR(A,hv) = TMR(A,hv) \times BSF(A,hv) \qquad (4\text{-}8)$$

The experimental setup for *BSF*, *TMR* and *TAR* is shown schematically in Figure, 4-6.

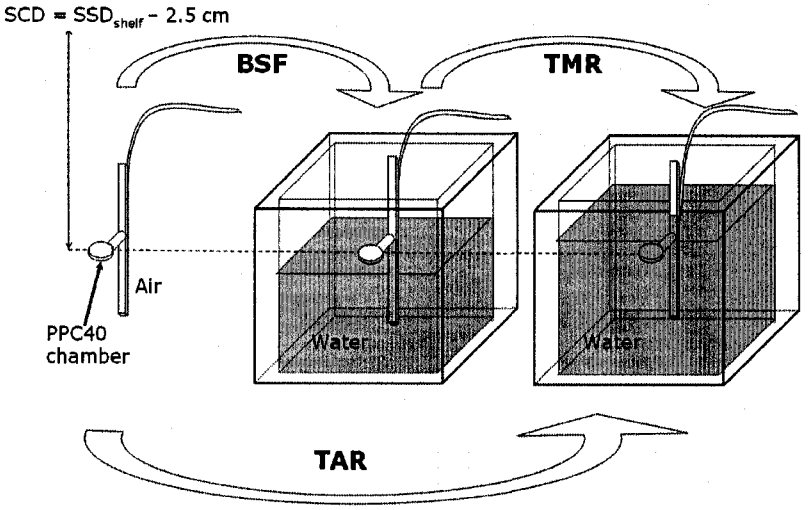

Figure 4-6: Schematic drawing of the BSF, TMR and TAR measurements setup.

A percentage depth dose (*PDD*) measurement was performed for the 160 kVp 0.5 mm Cu filtered beam at SSD = 29 cm using the small water tank. The tank was first filled up with water to the surface of the PPC40 chamber, then the chamber was moved to various depths down to 3 cm depth. The readings were corrected for temperature changes.

4.5.4 Irradiation Procedure for Small Animals

A procedure was developed for the irradiation and dose calculation formalism with respect to small animal experiments. Tables of outputs and *TAR*s were generated for irradiations to be performed at several source to axis distances (SAD = 20.4, 30.5 and 40.7 cm) with the 160 kVp 0.5 mm Cu filtered beam. The calculation formalisms involves the following steps:

1- Determination of the dose at a reference point where the output can be determined. e.g., center of "mouse" at z_{max} or in Air. (D_{ref})

2- Determination of the output at the reference point. (O_{ref})

3- Determination of irradiation time. $(t = \frac{D_{ref}}{O_{ref}})$

The formalism is illustrated in Figure 4-7. In Figure 4-7 (a), the formalism using the *TAR* function is shown: step (1) is to convert the prescribed or target dose (*TD*) to the reference point, which is at the center of "mouse" in air, by dividing by *TAR*; step (2) is to convert the output in air (dose rate) to the reference point by multiplying by an inverse square factor; and step (3) is calculating the time required for irradiation by dividing the dose at reference point (D_{ref}) by the output at reference point (O_{ref}). Alternatively, one can use the *PDD* function as illustrated in Figure 4-7 (b): step (1) is to convert the target dose (*TD*) to the reference point, which is at the surface of mouse (z_{max}), by dividing by *PDD*; step (2) is to first convert the output in air to the same SSD as the reference point by multiplying by an inverse square factor, and then to convert the output to the reference point by multiplying by *BSF*; and step (3) the time required for irradiation is calculated by dividing the dose at reference point (D_{ref}) by the output at reference point (O_{ref}).

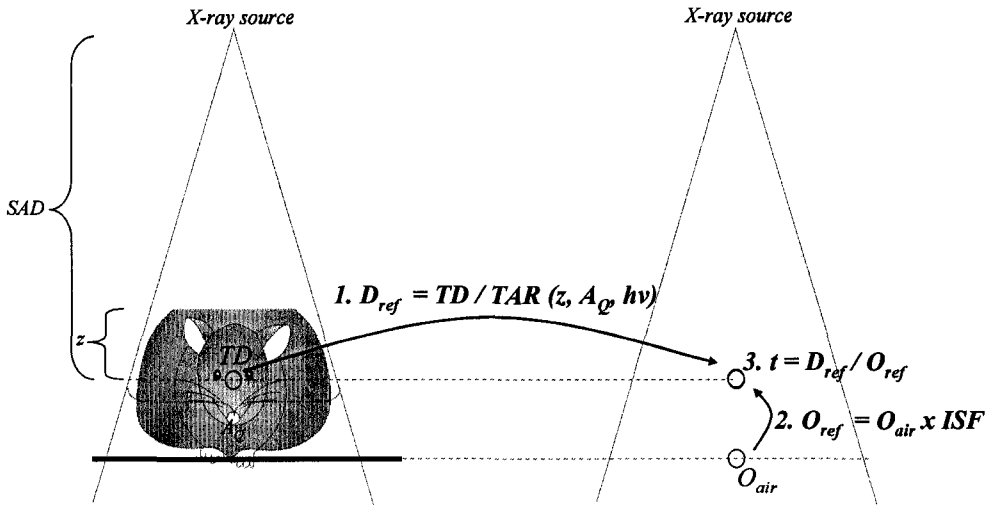

(a) using *TAR* function

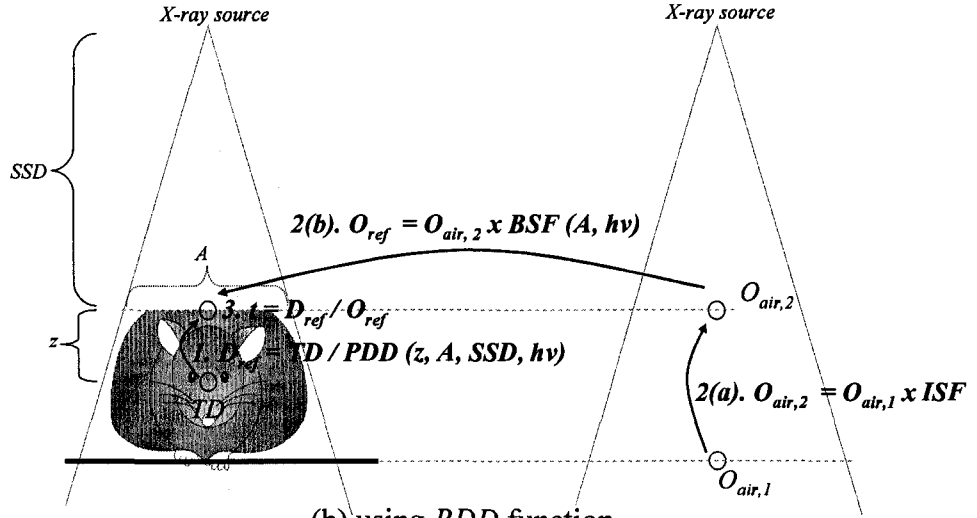

(b) using *PDD* function

Figure 4-7: Illustrations of the formalism used for mouse irradiation: (a) using TAR function, and (b) using PDD function.

Experiments were performed under a given "experimental" geometry to validate our formalisms. The mouse phantom described in Section 4.3 (length 7 cm, width 3 cm, height 3 cm) was placed at source to center of mouse distances (SAD) = 20.4, 30.5, and 40.7 cm. The mouse phantom was surrounded by PMMA in each case to produce full scattering conditions. The time needed to deliver 100 cGy at mouse center using the 160

kVp 0.5 mm Cu filtered beam with current setting of 6 mA was calculated, and a measurement with the NE2571 chamber was taken to validate the formalism. The dose delivered as read by the NE2571 chamber was computed using the AAPM TG-61 protocol's In-Phantom method for absolute dose determination.

For the specific case where the mouse is similar in size to our mouse phantom (length 7 cm, width 3 cm, height 3 cm), the dose rate at the center of the mouse can be found using AAPM TG-61 protocol's In-Phantom method:

$$\dot{D} = \dot{M} \times N_K \times P_{Q,cham} \times \left[\left(\frac{\bar{\mu}_{en}}{\rho} \right)_{air}^{w} \right]_{water} \qquad (4\text{-}9)$$

where $\dot{M}$ is the chamber reading at the center of mouse phantom corrected for temperature and pressure; N_K is the air kerma calibration coefficient for the given beam's quality; $P_{Q,cham}$ is the overall chamber correction factor that accounts for the change in the chamber response in the phantom compared to that for the calibration in air; and $\left[\left(\bar{\mu}_{en} / \rho \right)_{air}^{w} \right]_{water}$ is the ratio for water-to-air of the mean mass energy-absorption coefficients, averaged over the photon spectrum at the reference point in water. The calibration was performed using this method for the case where only the phantom is present, and also for the case where the phantom is surrounded by scattering materials (total of 10×10 cm^2 large phantom) to obtain an increased output.

4.6 References

1 Faxitron X-ray Corporation, *43855F Cabinet X-ray System Technical Manual, CP160 Option*

2 R. Gastorf, L. Humphries, and M. Rozenfeld, "Cylindrical chamber dimensions and the corresponding values of A_{wall} and $N_{gas}/(N_x A_{ion})$", Med Phys **13** (5), 751-754 (1986).

3 R. C. Tailor, W. F. Hanson, N. Wells et al., "Consistency of absorbed dose to water measurements using 21 ion-chamber models following the AAPM TG51 and TG21 calibration protocols", Med Phys **33** (6), 1818-1828 (2006).

4 E. B. Podgorsak (Editor), *Radiation Oncology Physics : A Handbook for Teachers and Students*. (International Atomic Energy Agency, Vienna, 2005).

5 M. J. Butson, T. Cheung, and P. K. Yu, "Weak energy dependence of EBT gafchromic film dose response in the 50 kVp-10 MVp X-ray range", Appl Radiat Isot **64** (1), 60-62 (2006).

6 S. Devic, J. Seuntjens, E. Sham et al., "Precise radiochromic film dosimetry using a flat-bed document scanner", Med Phys **32** (7), 2245-2253 (2005).

7 J. H. Hubbell and S. M. Seltzer, Tables of X-Ray Mass Attenuation Coefficients and Mass Energy-Absorption Coefficients from 1 keV to 20 MeV for Elements Z = 1 to 92 and 48 Additional Substances of Dosimetric Interest NISTIR 5632. National Institute of Standards and Technology (NIST).

8 C. G. Orton and J. B. Seibert, "The measurement of teletherapy unit timer errors", Phys Med Biol **17** (2), 198-205 (1972).

[9] C. M. Ma, C. W. Coffey, L. A. DeWerd et al., "AAPM protocol for 40-300 kV x-ray beam dosimetry in radiotherapy and radiobiology", Med Phys **28** (6), 868-893 (2001).

[10] "Central axis depth dose data for use in radiotherapy, BJR Supplement no. 25", Br. J. Radiol, (1996).

CHAPTER 5

RESULTS AND DISCUSSION

5.1 Dosimetric Characterization

5.1.1 Radiation Survey

The radiation survey showed that the radiation exposure around the irradiator is comparable to the background level. The maximum exposure rate detected was 12 μR/hr at about 15 cm from the lead window in front of the irradiator. The measured background was 11 μR/hr.

5.1.2 Radiation Field-Tray Marking Correspondence

The correspondence check, as shown in Figure 5-1, indicates there is a shift in the tray's marking of about 2.4 cm in the -Y direction. The shift in the X direction is negligible and can be minimized if the tray is positioned at the middle of the shelf holders.

The multi-irradiation image, Figure 5-1, shows that the field has the same center for the four upper trays. This indicates that the X-ray tube is shooting vertically and one can estimate the center of the beam by projecting the center of the focal spot perpendicularly. The image also indicates that the field is not completely circular. There is a sharp cut at the bottom (-Y direction) end of the circular field due to the collimation system of the X-ray tube.

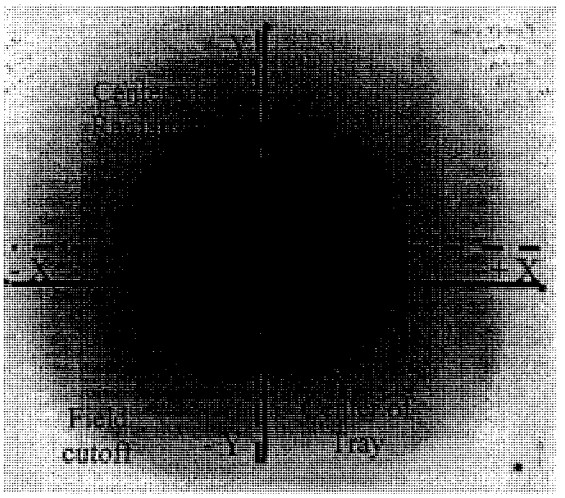

Figure 5-1: EDR2 film image indicating a shift in the -Y direction (about -2.4 cm) of the tray's marks as well as a sharp cutoff at the bottom of the circular field.

5.1.3 Beam Profile

The X axis (horizontal) and Y axis (vertical) profiles for the 160 kVp 0.5 mm Cu filtered beam at shelf #9 (SSD = 12.7 cm, field diameter = 10.3 cm) at the surface of the turntable is shown in Figure 5-2. The heel effect can be seen clearly at the -Y direction which corresponds to the anode side of the X-ray tube. Within a 5 cm diameter, the dose drops to 90% of the maximum, and to 80% within a 8 cm diameter in the X axis direction. However, the heel effect restricts the 90% of maximum dose area to within a 4 cm diameter and the 80% to within a 7 cm diameter in the Y direction.

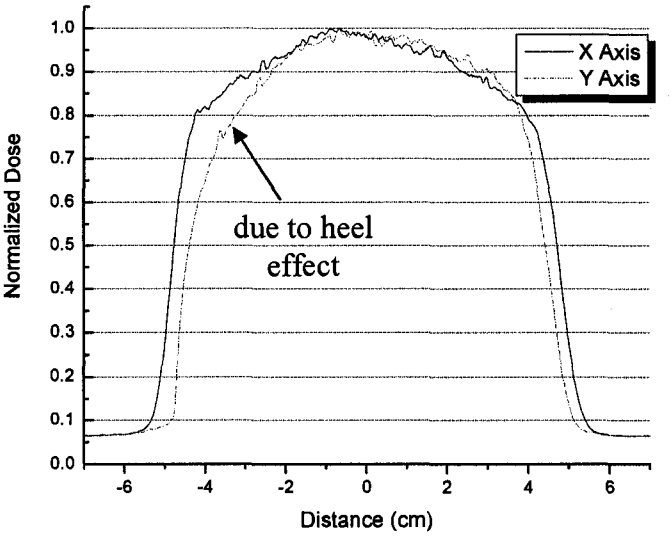

Figure 5-2: Dose profiles measured at the surface of turntable at shelf #9 (SSD = 12.7 cm) for the 160 kVp 0.5 mm Cu filtered beam.

At the center of a 3 cm thick Solid Water phantom, as shown in Figure 5-3, the dose drops to 90% within a 4 cm diameter and to 80% of the maximum dose within a 6 cm diameter.

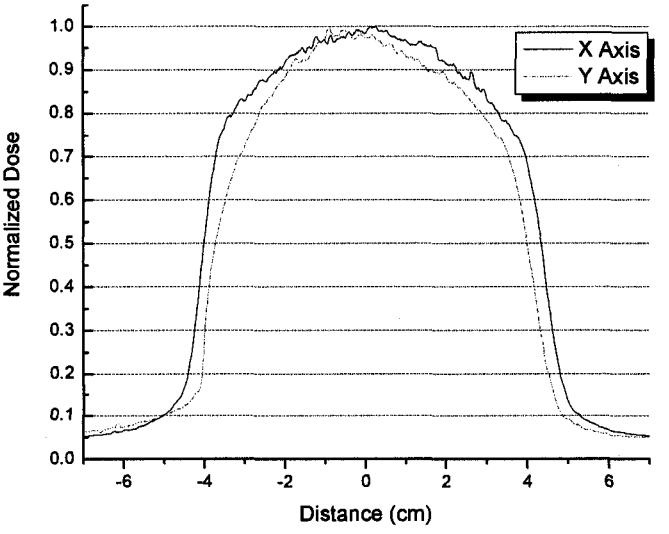

Figure 5-3: Dose profiles at the center of a 3 cm thick Solid Water phantom placed at shelf #9 (SSD = 12.7 cm) for the 160 kVp 0.5 mm Cu filtered beam.

The fact that the center of the company tray is different than the central axis of the X-ray beam results in a worse profile in terms of uniformity when rotating the turntable. Another noticeable effect of the off-centered rotation is the broadening of the dose profile, as shown in Figure 5-4.

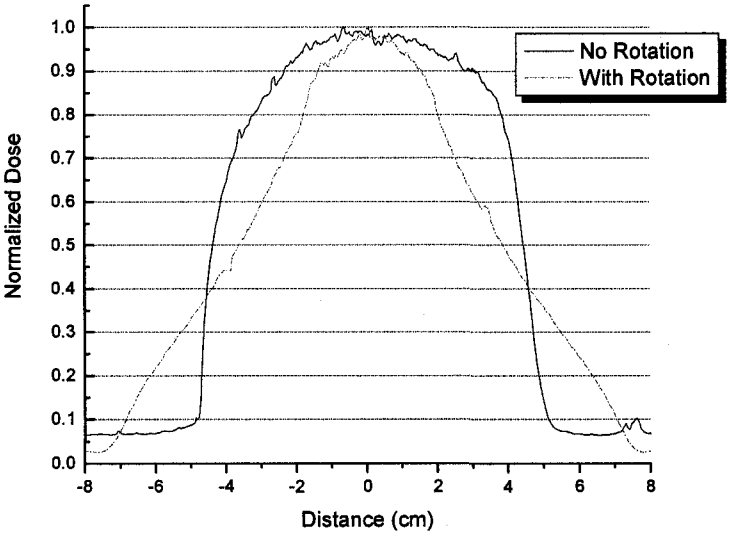

Figure 5-4: Y-Axis dose profiles at shelf #9 (SSD = 12.7 cm) with and without turntable rotation for the 160 kVp 0.5 mm Cu filtered beam.

5.1.4 Half-Value Layers and Effective Energies

The following tables, 5-1, 5-2, and 5-3, show the half-value layers and effective energies for the measured 0.5 mm Cu filtered, 0.5 mm Al filtered and non-filtered beams, respectively. The 160 kVp beam ranges, depending on the filtration, from a medium quality of 0.7 mm Cu (about 70 keV effective energy), low quality of 2.2 mm Al (about 30 keV), to a very low quality of 0.1 mm Al (about 10.6 keV).

kVp	1st *HVL* (mm Cu)	2nd *HVL* (mm Cu)	*HC*	E_{eff} (keV)
160	0.7	1.21	0.58	69.0
140	0.6	0.93	0.64	65.0
120	0.49	0.7	0.70	60.1
100	0.38	0.53	0.72	54.8

Table 5-1: For the 0.5 mm Cu filtered beam energies, values of the first and second half-value layers in mm Cu, homogeneity coefficient and effective energy using the NIST database.[1]

kVp	1st *HVL* (mm Al)	2nd *HVL* (mm Al)	*HC*	E_{eff} (keV)
160	2.24	5.59	0.40	29.8
140	1.81	4.21	0.43	27.5
120	1.50	3.33	0.45	25.6
100	1.20	2.53	0.47	23.7
80	0.96	1.83	0.53	21.9
60	0.74	1.28	0.58	20.0
40	0.54	0.83	0.65	17.9
20	0.23	0.31	0.74	13.4

Table 5-2: For the 0.5 mm Al filtered beam energies, values of the first and second half- value layers in mm Al, homogeneity coefficient and effective energy using the NIST database.[1]

kVp	1st *HVL* (mm Al)	2nd *HVL* (mm Al)	*HC*	E_{eff} (keV)
160	0.113	0.263	0.43	10.6
140	0.106	0.208	0.51	10.3
120	0.101	0.184	0.55	10.1
100	0.097	0.160	0.60	10
80	0.091	0.14	0.65	9.8
60	0.087	0.128	0.68	9.6
40	0.082	0.12	0.70	9.5
20	0.068	0.097	0.70	8.9

Table 5-3: For the non-filtered beam energies, values of the first and second half-value layers in mm Al, homogeneity coefficient and effective energy using the NIST database.[1]

5.1.5 Chamber Calibration

The air kerma and exposure calibration coefficients for the Faxitron CP160 beams resulting from cross-calibrating the NE2571 farmer chamber under both superficial and orthovoltage beams are shown in Figure 5-5 and in Table 5-4.

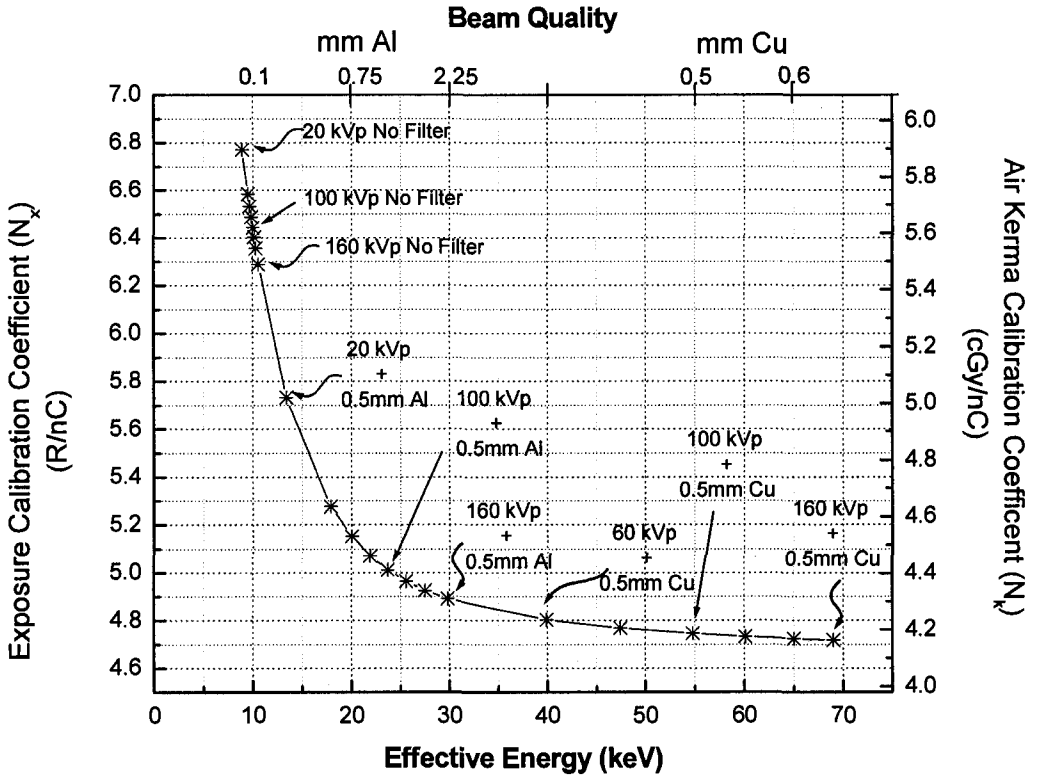

Figure 5-5: Calibration curve for the NE2571 chamber showing air kerma and exposure calibration coefficients for the Faxitron CP160 beams.

Filtration	kVp	*HVL* (mm Al)	E_{av} (keV)	N_X (R/nC)	N_K (cGy/nC)	$\left(\frac{\mu_{en}}{\rho}\right)^{w}_{air}$
0.5 mm Cu Filter	160	10.43	69.0	4.717	4.143	1.062
	140	9.46	65.0	4.723	4.149	1.056
	120	8.58	60.1	4.732	4.157	1.049
	100	7.59	54.8	4.745	4.168	1.041
	80	6.34	47.4	4.768	4.187	1.036
	60	4.50	39.9	4.803	4.215	1.027
0.5 mm Al Filter	160	2.24	29.8	4.891	4.288	1.019
	140	1.81	27.5	4.926	4.317	1.018
	120	1.50	25.6	4.964	4.349	1.017
	100	1.20	23.7	5.012	4.390	1.018
	80	0.96	21.9	5.072	4.442	1.020
	60	0.74	20.0	5.153	4.513	1.023
	40	0.54	17.9	5.276	4.621	1.027
	20	0.23	13.4	5.733	5.025	1.038
No Filter	160	0.113	10.56	6.289	5.511	1.043
	140	0.106	10.29	6.355	5.569	1.044
	120	0.101	10.11	6.404	5.611	1.044
	100	0.097	9.96	6.443	5.645	1.044
	80	0.091	9.80	6.488	5.684	1.044
	60	0.087	9.65	6.532	5.723	1.044
	40	0.082	9.47	6.585	5.769	1.044
	20	0.068	8.88	6.771	5.931	1.042

Table 5-4: Exposure calibration coefficients (N_X) and air kerma calibration coefficients (N_K) for the beams generated by the Faxitron CP160. The table also shows HVL values in mm Al, the effective energies and the ratios of average mass energy-absorption coefficients water to air, free in air, to convert air kerma to water dose in air.

5.1.6 Measured Outputs

The measured outputs in air at source-chamber distance (SCD) = 33 cm and current setting of 6 mA are shown in Table 5-5 below. The water dose rate ranges

between about 1400 cGy/min for a non-filtered beam and 2 cGy/min for a 0.5 mm Cu filtered beam.

Filter	No filter		0.5 mm Al		0.5 mm Cu	
kVp	Water Dose Rate in Air (cGy/min)	Exposure Rate (R/min)	Water Dose Rate in Air (cGy/min)	Exposure Rate (R/min)	Water Dose Rate in Air (cGy/min)	Exposure Rate (R/min)
160	1393.1	1523.7	193.1	216.3	48.0	51.4
150	1397.8	1528.4	181.5	203.3	40.7	43.6
140	1395.1	1525.5	170.1	190.7	34.1	36.8
130	1388.6	1517.5	159.0	178.4	28.2	30.4
120	1372.0	1499.9	147.3	165.3	22.7	24.7
110	1348.0	1473.8	135.8	152.4	17.5	19.0
100	1315.9	1438.5	124.3	139.4	13.1	14.3
90	1271.9	1390.7	111.7	125.2	9.2	10.0
80	1207.1	1319.6	99.8	111.7	6.1	6.8
70	1128.0	1233.2	86.5	96.8	3.6	4.0
60	1020.6	1115.9	72.3	80.7	1.9	2.2
50	865.8	947.2	58.0	64.7		
40	695.9	760.8	42.1	46.8		
30	476.1	523.8	24.0	26.9		
20	214.7	235.1	6.9	7.6		

Table 5-5: In air measured outputs, water dose rates in air and exposure rates, at source-chamber distance (SCD) of 33 cm, and current setting of 6 mA for the Faxitron CP160 irradiator.

5.1.7 Output Constancy

a) Output Reproducibility: The experiment was performed at 160 kVp and 6.3 mA and repeated 20 times. The same experiment was also performed at 100 kVp and 10 mA. For both experiments the results were normalized to the average dose measured. The normalized dose ranged between 1.001 and 0.999 and the standard deviation was 0.001.

b) Long Term Constancy: The output was monitored for 46 days for the 160 kVp and 6 mA. The results were normalized to the average dose measured. The normalized dose

ranged between 1.013 and 0.984 and the standard deviation was 0.012. Figure 5-6 shows the data for this experiment.

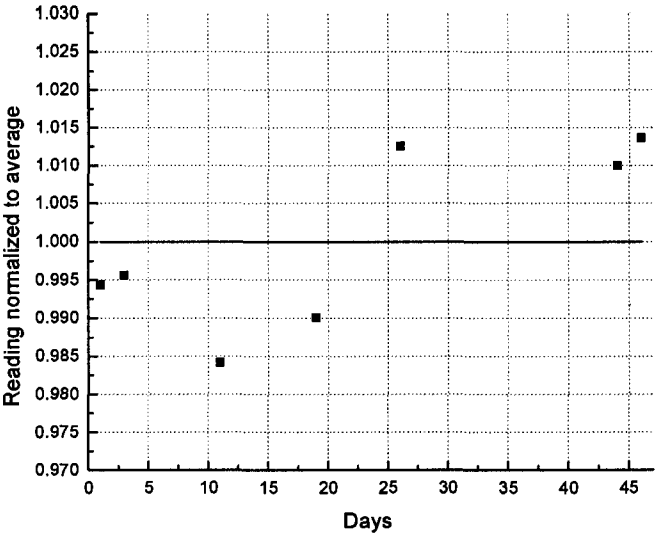

Figure 5-6: Output constancy during a period of 46 days. The experiment was performed on top of turntable at 32 cm SSD using 160 kVp and 6 mA technique.

c) Constancy during Prolonged Exposure: The experiment was performed with the 160 kVp (max kVp) beam and current setting of 6.3 mA (max mA) for 30 minutes. The results were normalized to the average dose rate measured. The normalized dose rate ranged between 1.0008 and 0.9989 and the standard deviation was 0.0004. Figure 5-7 shows the data for this experiment.

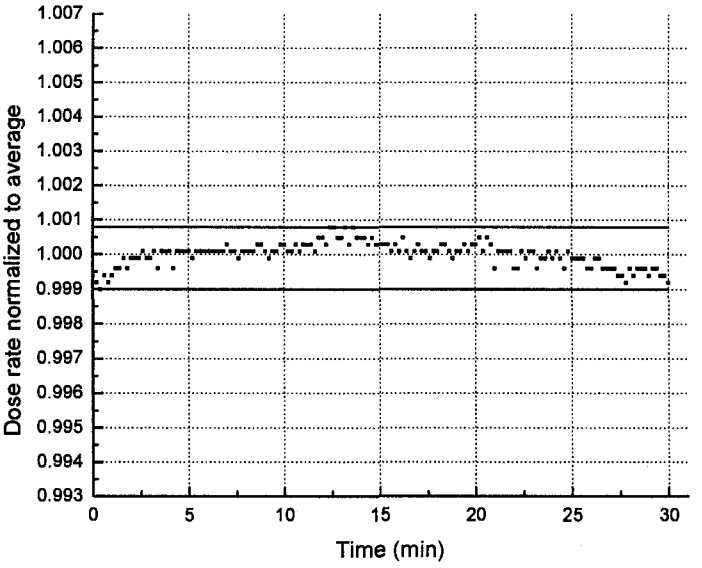

Figure 5-7: Output constancy during prolong exposure. The experiment was performed in air at 32 cm SCD using 160 kVp and 6.3 mA technique.

5.1.8 Absolute Output vs. kVp

The output vs. kVp relationship is shown in Figure 5-8. We do not expect to have the same relationship for the different filtrations since a non-filtered beam has more low energy photons that are preferentially attenuated compared to a filtered beam which has more penetrative high energy photons yielding a complex relationship between output and kVp.

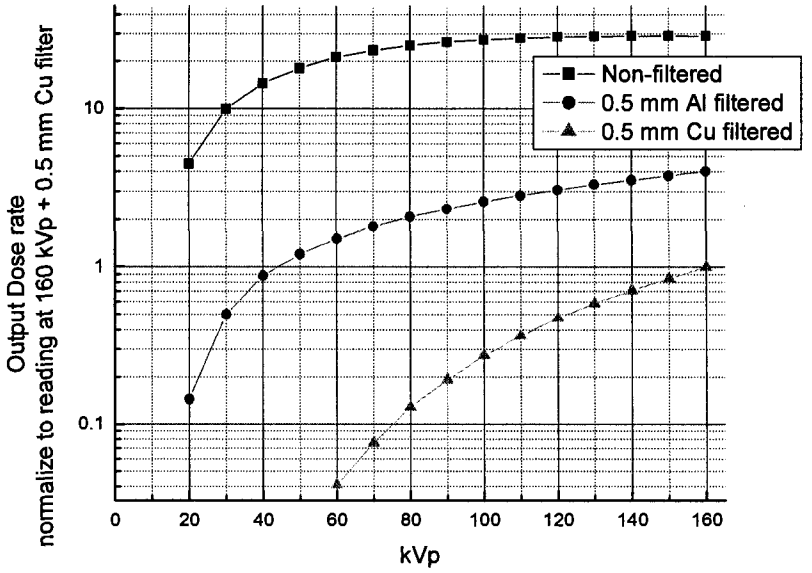

Figure 5-8: Output vs. kVp for the three160 kVp qualities. The measurements were performed in air at 33 cm SCD for current setting of 6 mA.

5.1.9 Relationship between Output, mA and Time

The output vs. mA relationship for both the 160 kVp and 100 kVp beams are shown in Figure 5-9 for the three beam qualities. The relationship between output and mA is linear for the beam qualities measured.

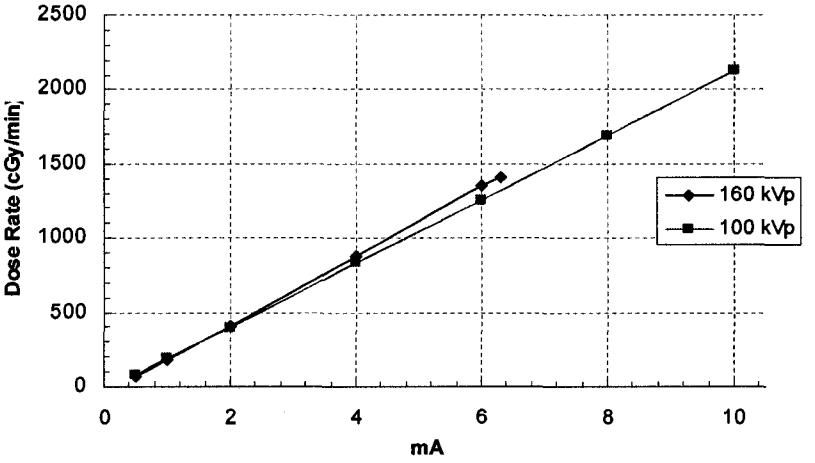

(a) No filtration, SCD = 34 cm.

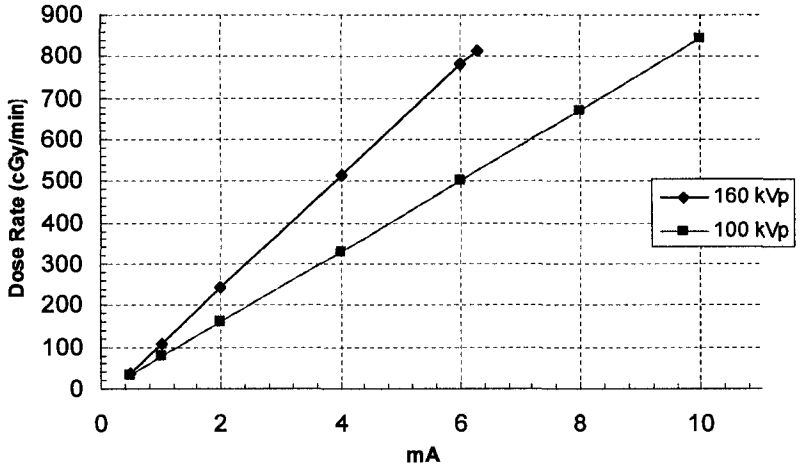

(b) 0.5 mm Al filtration, SCD = 16.7 cm.

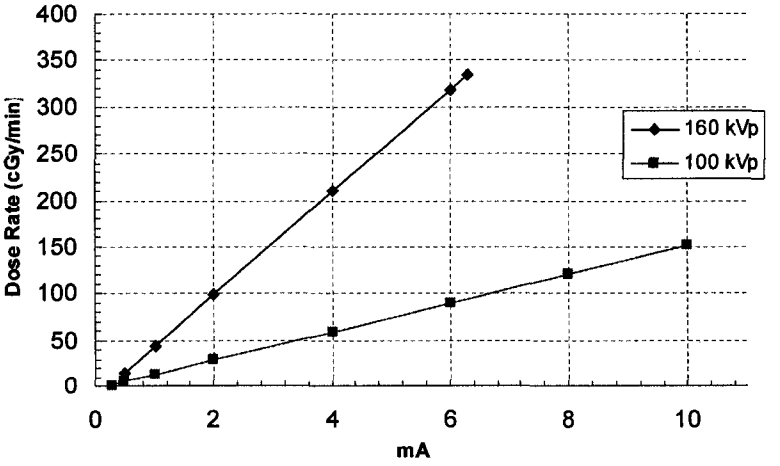

(c) 0.5 mm Cu filtration, SCD = 12.8 cm.

Figure 5-9: Output vs. mA for the 160 kVp and 100 kVp beams with (a) no filtration, (b) 0.5 mm Al filtration, and (c) 0.5 mm Cu filtration. The measurements were performed in air.

The experiment for the output with time showed a linear relationship as seen in Figure 5-10.

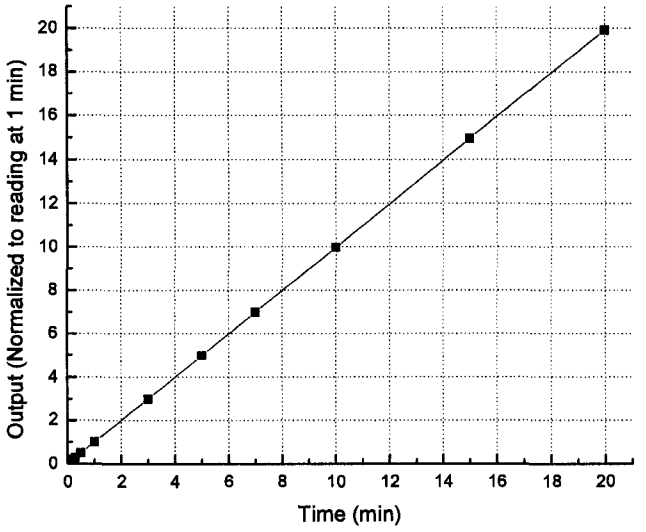

Figure 5-10: Output vs. time showing a linear relationship. The measurement was performed in air at 33 cm SCD using the 160 kVp 0.5 mm Cu filtered beam with 6 mA.

5.1.10 Output Reciprocity with mAs

Below a 3 mA setting, the reciprocity of mA and time does not hold, indicating that different combinations of mA and time to produce the same mAs can give different outputs as shown in Table 5-6. The deviation can be as high as 10% when using low mA (~ 1 mA). Generally however, for a higher mAs settings the output reciprocity holds. If the mA readout is assumed to be overestimating by 0.1 mA, then the output deficiency at 3 mA is 3% (=(1-3/2.9) in percentage). At 2 mA the deficit is 5%, and at 1 mA it is 11%. This agrees with the measured deficiencies in output as shown in Table 5-6.

Beam Quality	mAs	mA	Time (min)	Relative Output
160 kVp + 0.5 mm Cu Filter	1800	3	10	0.97
		5	6	1.00
		6	5	1.00
100 kVp + 0.5 mm Cu Filter	600	1	10	0.90
		2	5	0.95
		4	2.5	0.98
		5	2	0.99
		10	1	1.00
	1200	2	10	0.95
		4	5	0.99
		5	4	1.00
		10	2	1.00
	1800	3	10	0.97
		5	6	0.99
		10	3	1.00
	2400	2	20	0.96
		5	8	0.99
		10	4	1.00

Table 5-6: Results for the reciprocity test for the 0.5 mm Cu filtered beam with technique used shown. The outputs are normalized to the readings of the highest mA settings.

5.1.11 Shutter Error

The shutter error, using the double exposure method described in Section 4.4.11, was found to be 0.3 seconds. Note that the smallest interval the time can be set to is 0.1 min (6 seconds), and that the setting is not on a continuous scale, therefore a correction for shutter error is not possible. For a 0.5 min (30 sec) irradiation, this would result in a 1% timer error.

5.1.12 Inverse Square Law

The deviation from the inverse square law for the three 160 kVp quality beams is shown in Figure 5-11. As can be seen from the graph, the inverse square law underestimates the expected output for short source-chamber distances (SCD) since we have contribution of excessive radiation from the collimator and other scattering surfaces in the unit. For long SCDs and low quality beams, on the other hand, the inverse square law overestimates the expected values due to the attenuation of low energy photons in air, which is more emphasized for the non-filtered beam.

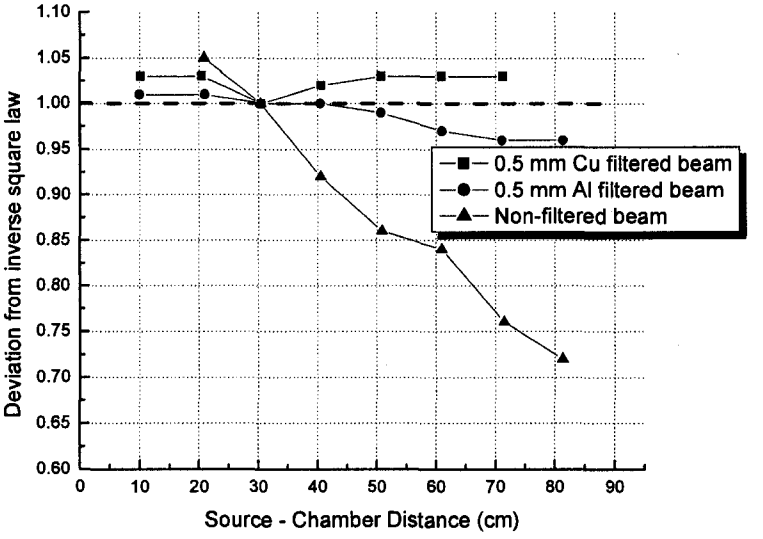

Figure 5-11: The deviation from the inverse square law for the three quality beams. Measurements were done at 160 kVp. The (output × SCD^2) values were normalized arbitrarily to SCD = 30 cm.

Around shelf #7, SCDs between 28 and 38 cm, the inverse square law was found to be valid within 1% for the 160 kVp 0.5 mm Cu filtered beam. This is very relevant for the calculation formalism developed later on in this work for small animal irradiations.

5.1.13 Tray Factors

Tray factors (i.e., the change in output due to the backscattering from the tray beneath the specimen) for different shelf positions under 160 kVp beam are shown in Table 5-7. The factors were measured for the company tray with its turntable on top.

Filtration	Shelf #	SSD (cm)	Tray Factor
0.5 mm Cu	9	11.7	1.07
	8	21.9	1.14
	7	32	1.18
0.5 mm Al	7	32	1.1
No Filter	7	32	1.03

Table 5-7: Tray factors for different shelf positions. Values are quoted for the 160 kVp beam.

The tray factor increases with increasing field size (i.e., decreasing shelf position) because of the increasing photon scatter. For the same field size (shelf #7), the backscatter is largest at the highest quality beam (160 kVp 0.5 mm Cu filtered) in our case as expected from theory. For low beam qualities, the backscattered photon energy is small and most photons are likely to get absorbed in the tray material before reaching the detector.

5.2 Operational Commissioning

5.2.1 Outputs on Tray for Cell Irradiation Configuration

Tables 5-8 summarizes the water dose rates in air and exposure rates on the tray to be used for cell cultural irradiations for the 160 kVp - 6 mA and the 100 kVp - 10 mA techniques.

Filtration	Shelf #	SSD (cm)	160 kVp – 6 mA		100 kVp - 10 mA	
			Water Dose Rate in Air (cGy/min)	Exposure Rate (R/min)	Water Dose Rate in Air (cGy/min)	Exposure Rate (R/min)
0.5 mm Cu	9	11.7	418.1	489.2	215.2	234.4
	8	21.9	126.2	141.8	61.9	67.8
	7	32	60.2	66.6	28.6	31.6
	6	42.2	35.3	38.7	16.5	18.4
0.5 mm Al	9	11.7	1624.9 (5 mA)	1985.7 (5 mA)	1051.7	1151.8
	8	21.9	479.2	561.9	535.3	587.1
	7	32	227.2	262.6	247.7	272.3
	6	42.2	131	150.3	141.4	156
No Filter	9	11.7	9882.6 (4 mA)	10809.1 (4 mA)	10888.4 (5 mA)	11618.4 (5 mA)
	8	21.9	3408.5	3904.3	5749.7	6136.9
	7	32	1523.6	1719.7	2480.7	2648.7
	6	42.2	795.3	890.8	1291.2	1379.4

Table 5-8: Outputs on tray (in air measurements) a the upper four shelf positions for the techniques indicated.

The measured outputs at shelf #7 (SSD = 32 cm) for the Cu and Al filtered beams agree with the values quoted by the manufacturer within 5%. For the non-filtered beams, it was found that the measured values differs from the manufacturer's by up to 20%, probably due to the non-constant energy response of the chamber at these low quality energies and the difficulty in determining the half-value layers precisely.

5.2.2 Irradiation Procedure for Cell Cultures

The attenuation through the flask wall was not found to be significant for the 0.5 mm Cu filtered beam. For the 0.5 mm Al filtered beam, there was a small reduction of about 1% in dose when measuring inside the flask. For the non-filtered beam, the

attenuation was large as expected and it reduces the dose by about 23% because of its low penetrative quality. Theoretical estimation for beam attenuation using the exponential attenuation law for the beam qualities used passing through a 1 mm thick wall made of PMMA (elemental composition (% by mass): H (8%), C (60%), and O (32%), density = 1.17 g/cm^3)^2 yields 25% attenuation for the 160 kVp non-filtered beam, 4% for the 160 kVp 0.5 mm Al filtered beam, and 2% for the 160 kVp 0.5 mm Cu filtered beam. The discrepancy between theoretical calculations and measurements could be due to the fact that the wall is made of other material than PMMA.

To verify the irradiation procedure in a laboratory mode, Gafchromic EBT film measurements were performed for the 160 kVp 0.5 mm Cu filtered beam and current setting of 6 mA at the upper three shelves (SSD = 11.7, 21.9, and 32 cm). The values agree within 3% with the values shown in Table 5-8.

For the experimental setup verification, the time needed to deliver a target dose of 100 cGy to the cells placed on top of a $30\times30\times10$ cm^3 Solid Water phantom at SSD = 29 cm using 160 kVp 0.5 mm Cu filtered beam and current setting of 6 mA was found to be 1.1 minutes, taking into account the backscatter factor (1.39) for that field size (23.3 cm diameter). The dose measured with the Gafchromic film was within 4% of the target dose.

5.2.3 Dosimetric Functions: *BSF, TMR, TAR* and *PDD*

Backscatter factors (*BSF*) for the indicated shelf positions and beam qualities are shown in Table 5-9. The table also shows a comparison with the TG-61[3] protocol and BJR-25[4]. The measured *BSF* are up to 9% lower than the literature values, probably due to the attenuation of backscattering from the phantom by the parallel plate chamber body. Note that the maximum field diameter used in these two references is about 20 cm.

Beam Quality	Shelf #	SSD (cm)	Measured		TG-61		BJR-25	
			Field Diameter (cm)	*BSF*	Field Diameter (cm)	*BSF*	Field Diameter (cm)	*BSF*
0.5 mm Cu (HVL = 0.7 mm Cu)	8	20.4	16.5	1.35	15	1.41	16.7	1.44
	7	30.5	24.5	1.40	20	1.47	22.2	1.49
	6	40.7	33	1.43	20	1.48	22.2	1.49
0.5 mm Al (HVL = 2.2 mm Al)	7	30.5	24.5	1.23	20	1.29	22.2	1.30

Table 5-9: Backscatter factors (BSF) for the field sizes and beam qualities indicated. Values of BSF as extracted from TG-61 and BJR-25 for the nearest field sizes and SSDs are also shown for comparison.

Figure 5-10 shows tissue air ratio (*TAR*) and tissue maximum ratio (*TMR*) at shelf positions #8, 7, and 6 (source-axis distances (SADs) = 20.4, 30.5, and 40.7, respectively) for the 160 kVp 0.5 mm Cu filtered beam, and at shelf #7 (SAD = 30.5 cm) for the 160 kVp 0.5 mm Al filtered beam. For the 0.5 mm Cu filtered beam, an initial increase in *TAR* and *TMR* values is noticed. This is due to the photon scattering from surrounding water. Figure 5-10 (a) also shows *TAR* values as extracted from BJR-25 for a beam quality of 0.7 mm Cu and a field diameter of 22.2 cm for comparison with *TAR* values of the 160 kVp 0.5 mm Cu filtered beam at shelf # 7 (field diameter = 24.5 cm). The large differences in *TAR* values are due to the differences in backscatter factors between our measurements and tabulated values in the literature as seen in Table 5-9.

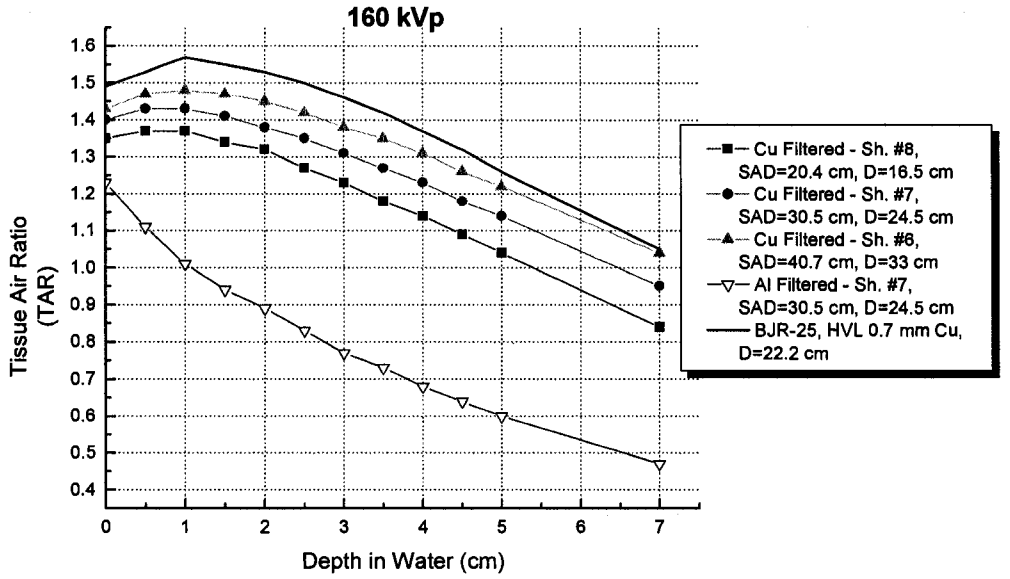

(a)

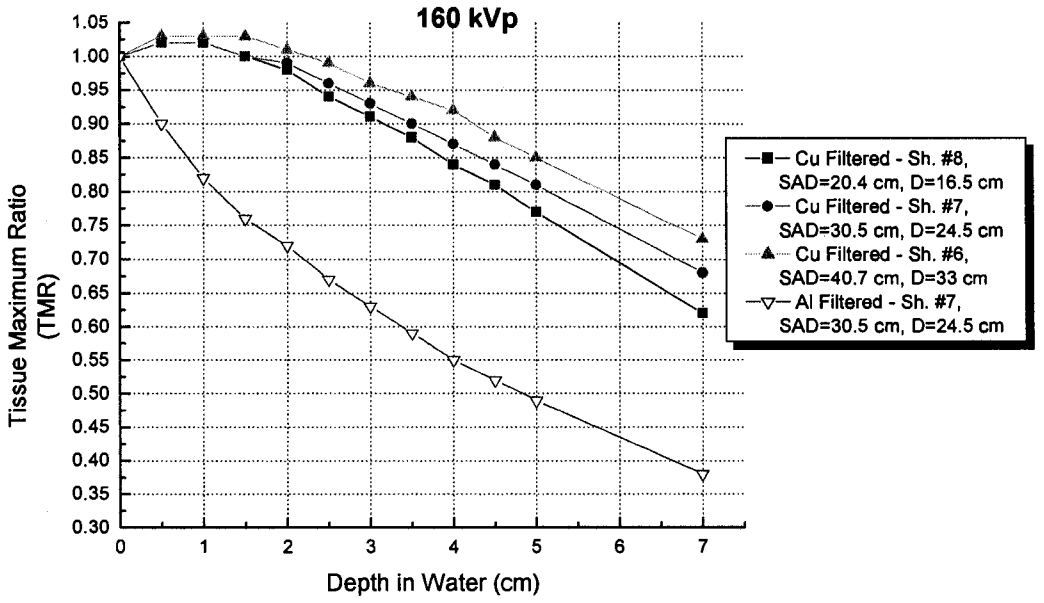

(b)

Figure 5-10: (a) Tissue air ratio and (b) tissue maximum ratio for the160 kVp beam for three shelf positions: # 8, 7 and 6 (for beam filtered with 0.5 mm Cu) and for shelf #7 (for beam filtered with 0.5 mm Al filter). Also shown in (a) TAR extracted from BJR-25 to be compared with the160 kVp 0.5 mm Cu filtered beam at shelf # 7.

Table 5-10 shows backscatter factors and some of the selected values of *TAR* for the indicated shelf positions and beam qualities. *BSF*, by definition, is the same as *TAR(0)* in superficial and orthovoltage beams. Also, one should keep in mind that these values apply to a large phantom, i.e., for a full scattering condition.

Filtration	Shelf #	SSD (cm)	Field Diameter (cm)	*TAR*				
				(*BSF*) 0 cm	1 cm	1.5 cm	2 cm	3 cm
0.5 mm Cu	8	20.4	16.5	1.35	1.37	1.34	1.32	1.23
	7	30.5	24.5	1.40	1.43	1.41	1.38	1.31
	6	40.7	33	1.43	1.48	1.47	1.45	1.38
0.5 mm Al	7	30.4	24.5	1.23	1.01	0.94	0.89	0.77

Table 5-10: Backscatter factors and selected tissue air ratio values for 160 kVp beam with 0.5 mm Cu filtration and with 0.5 mm Al filtration for the shelf positions indicated.

As one would expect from the theory, the *TAR* and *TMR* increase with increasing field size. Also, the 0.5 mm Al filtered beam is not as penetrating as the 0.5 mm Cu filtered beam and thus it will not yield as good dose uniformity along the animal body depth as the 0.5 mm Cu filtered beam.

Table 5-11 shows the percentage depth dose (*PDD*) for the 160 kVp 0.5 mm Cu filtered beam (HVL = 0.7 mm Cu) for both measurement and BJR-25 for comparison. The BJR-25 values in the protocol are given for SSD = 50 cm and field size of 22.6 cm diameter, and thus were corrected for SSD = 29 cm with field size of 23.3 cm diameter using Equation 2-12, with the *BSF* ratio assumed to be 1. The values of our measurement is in agreement within 1.5% of the values found in the literature.

Depth (z) (cm)	Measurement	BJR-25
	PDD (*SSD*=29 cm, Ø= 23.4 cm, z, 0.7 mm Cu)	*PDD* (*SSD*=29 cm*, Ø= 22.2 cm, z, 0.7 mm Cu)
0.0	100.0	100.0
0.3	99.9	99.5
0.5	99.2	99.2
1.0	97.0	98.4
1.5	93.7	94.3
2.0	89.9	90.2
2.5	86.4	85.8
3.0	82.2	81.4

Table 5-11: Percentage depth dose (PDD) for source-surface distance SSD=29 cm, field diameter of about 23 cm and beam quality of 0.7 mm Cu HVL (160 kVp 0.5 mm Cu filtered beam) for both measurement and BJR-25.

** PDD was corrected from SSD =50 cm to SSD = 29 cm using Equation 2-12.*

5.2.4 Irradiation Procedure for Small Animals

To validate our formalism for small animal irradiation, a mouse phantom (length 7 cm, width 3 cm, height 3 cm) was surrounded by PMMA to produce full scattering conditions. The time needed to deliver a target dose (*TD*) of 100 cGy at the mouse center for different source-axis distances using the 160 kVp 0.5 mm Cu filtered beam with current setting of 6 mA was calculated as shown in Table 5-12. The delivered dose was measured using the NE2571 chamber and it was within 5% from the target dose.

SAD (cm)	Target Dose (TD) (cGy)	z (cm)	TAR (1.5 cm)	$D_{ref} = \frac{TD}{TAR}$ (cGy)	O_{ref} (cGy/min)	Calc. Time $t = \frac{D_{ref}}{O_{ref}}$ (min)	Time Setting (min)	Meas. Dose (cGy)	% difference
20.4	100	1.5	1.34	74.63	125.61	0.59	0.6	94.9	5.1 %
30.5	100	1.5	1.41	70.92	56.19	1.26	1.3	101.1	1.1 %
40.7	100	1.5	1.47	68.03	31.56	2.16	2.2	100.8	0.8 %

Table 5-12: Parameters and results for irradiating a 3 cm thick mouse phantom at different source-axial distances (SAD) with 160 kVp 0.5 mm Cu filtered beam and current setting of 6 mA to deliver a target dose of 100 cGy at mouse center.

Absolute output measurements were also done inside a small mouse phantom following the TG-61[3] In-Phantom method (Equation 4-9), with $\left[\left(\frac{\overline{\mu}_{en}}{\rho}\right)^{w}_{air}\right]_{water}$ equals to 1.053, and $P_{Q,cham}$ equals to 1.027, taking into account the $P_{Q,cham}$ dependence on field size (0.25%), for the 160 kVp beam used (HVL 0.7 mm Cu). These values, specified for a reference depth of 2 cm in the TG-61 protocol, are taken as estimation for the values of our measurement point at 1.5 cm depth in phantom. The results are shown in Table 5-13. Note that this table is to be used for the special case where the mouse is similar in size to our mouse phantom (length 7 cm, width 3 cm, height 3 cm) and full scattering conditions do not exist.

Filtration	Shelf #	SAD (cm)	Field Diameter (cm)	Dose Rate (cGy/min)
0.5 mm Cu	8	20.4	16.5	136.9
	7	30.5	24.5	63.2
	6	40.7	33	37.3

Table 5-13: Absolute does outputs at the center of a small mouse phantom (length 7 cm, width 3 cm, height 3 cm) using TG-61 In-Phantom method. Values are quoted for the160 kVp 0.5 mm Cu filtered beam and 6 mA.

If one is to use scattering material around the mouse to make a total size of about 10×10 cm^2, then the dose output is increased because of the increased scattered radiation and this reduces the time of irradiation by about 20%. Table 5-14 is to be used in this case.

Filtration	Shelf #	SAD (cm)	Field Diameter (cm)	Dose Rate (cGy/min)
0.5 mm Cu	8	20.4	16.5	158.4
	7	30.5	24.5	73.8
	6	40.7	33	42.4

Table 5-14: Absolute dose outputs at the center a small mouse phantom surrounded by scattering material (total size of about 10×10 cm^2) using TG-61 In-Phantom method. Values are quoted for the160 kVp 0.5 mm Cu filtered beam and 6 mA.

Note that if a very short time is required to deliver the dose, then a shelf position further from the source increasing the time could yield a higher precision in dose delivery since the minimum timer setting is 0.1 minutes. Alternatively, the user could calculate the

dose delivered given a settable time. For example, a calculated time of 1.05 minutes would result in a setting of 1.1 minutes yielding a dose 5% higher than expected.

5.3 References

[1] J. H. Hubbell and S. M. Seltzer, Tables of X-Ray Mass Attenuation Coefficients and Mass Energy-Absorption Coefficients from 1 keV to 20 MeV for Elements Z = 1 to 92 and 48 Additional Substances of Dosimetric Interest NISTIR 5632, National Institute of Standards and Technology (NIST).

[2] J. Zoetelief, J. J. Broerse, R. W. Davies et al., "Protocol for X-ray dosimetry in radiobiology", Int J Radiat Biol **77** (7), 817-835 (2001).

[3] C. M. Ma, C. W. Coffey, L. A. DeWerd et al., "AAPM protocol for 40-300 kV x-ray beam dosimetry in radiotherapy and radiobiology", Med Phys **28** (6), 868-893 (2001).

[4] "Central axis depth dose data for use in radiotherapy, BJR Supplement no. 25", Br. J. Radiol, (1996).

CHAPTER 6

CONCLUSION

6.1 Summary

Kilovoltage radiobiological irradiator units used for research have many advantages over linear accelerators and Co-60 machines, such as the low cost, small equipment size, easy maintenance, more accessibility and less stringent licensing requirements. The Faxitron CP160 X-ray irradiator is a commercially available kilovoltage radiobiological irradiator. The main objective of this thesis was to commission the Faxitron CP160 X-ray irradiator to make it usable for cells and small animal total body irradiation.

The reference dosimetry was performed following the recommendations of the AAPM TG-61 protocol, and using a cylindrical ionization chamber model NE2571 with Keithley 35617 digital electrometer calibrated in air in terms of air kerma under a kilovoltage beam.

6.2 General Use of the Faxitron CP160 Irradiator

Based in the results of this work, the following are general observations and recommendations for using the Faxitron CP160 irradiator:

- The generated beams were found to range between HVL 0.7 mm Cu for a 160 kVp 0.5 mm Cu filtered beam, and HVL 0.07 mm Al for a 20 kVp non-filtered beam.

- Although all beam dose rates were measured, only the 160 kVp and 100 kVp beams were fully characterized.
- All beams deliver their maximum dose at the surface.
- The highest dose rate in air at shelf position #7 (source-chamber distance = 33 cm) and tube current setting of 6 mA is 1398 cGy/min (exposure rate = 1529 R/min) using the 150 kVp non-filtered beam. All non-filtered beams above 130 kVp yield the same output within 1%.
- The most penetrating beam is the 160 kVp 0.5 mm Cu filtered beam. The percentage depth dose (*PDD*) at depth 1, 2, and 3 cm is 97%, 89.9% and 82.2%, respectively.
- The 160 kVp 0.5 mm Cu filtered beam with current setting of 6 mA yields a dose rate in air of 48.0 cGy/min (exposure rate = 51.4 R/min) at a source-chamber distance of 33 cm.
- The 160 kVp 0.5 mm Al filtered beam with current setting of 6 mA yields a dose rate in air of 193.1 cGy/min (exposure rate = 216.3 R/min) at a source-chamber distance of 33 cm. The dose rate produced by this beam is similar to that using a conventional Linac or Co-60 unit for irradiations.
- For low dose rate irradiations, we recommend the use of the 100 kVp 0.5 mm Cu filtered beam with current setting of 10 mA at a source-chamber distance of 33 cm yielding a dose rate in air of 13.1 cGy/min (exposure rate = 14.3 R/min).

6.3 Cell Cultures Irradiation using the Faxitron CP160 Irradiator

For cell cultures irradiations, outputs on tray were determined for both the 160 kVp – 6 mA and the 100 kVp – 10 mA techniques for the 0.5 mm Cu filtered, 0.5 mm Al filtered and non-filtered beams. The dose to the cell cultures inside a flask can be assumed to be equal to these outputs for the 0.5 mm Cu and the Al filtered beams, and the irradiations using these beams are valid within 4%. The following are recommendations for using the Faxitron CP160 irradiator for cell cultures irradiations:

- The specimen is recommended to be placed on the company tray at center of beam field at shelf position #7 (SSD = 32 cm) with the turntable switched off.
- For thick wall (>1 mm) flasks, the 160 kVp 0.5 mm Cu filtered with current setting of 6 mA should be used. The beam output using this technique is 60.2 cGy/min (66.6 R/min).
- For thin wall (<1 mm) flasks, the 160 kVp 0.5 mm Al filtered with current setting of 6 mA can be used. The beam output using this technique is 227.2 cGy/min (262.6 R/min).
- The non-filtered beams should NOT be used for cell irradiations as the attenuation through the flask reduces the dose by up to 23% when comparing to outputs on tray.

6.4 Small Animals Irradiation using the Faxitron CP160 Irradiator

A calculation formalism was developed for small animal total body irradiations. The formalism involves calculating the dose at a reference depth (D_{ref}) at center of small

animal using a tissue air ratio (*TAR*) function, and calculating the output at that reference point (O_{ref}). The time needed for irradiation is then the ratio of D_{ref} to O_{ref}. The formalism was found to be valid within 5%. The following are recommendations for using the Faxitron CP160 irradiator for small animal total body irradiations:

- The small animal should be placed on the company tray at the center of the beam field at shelf position #7 (SSD = 32 cm) surrounded by scattering materials to produce full scattering conditions.
- The 160 kVp 0.5 mm Cu filtered beam with current setting of 6 mA is recommended because of its high penetrating power.
- The water dose rate in air using this technique is 56.2 cGy/min at source-axial distance (SAD) of 30.5 cm, the backscatter value is 1.4, and the tissue air ratio at depth 1, 1.5, and 2 cm are 1.43, 1.41 and 1.38, respectively.
- The inverse square law can be used to estimate the dose rate at source-axial distances between 28 and 38 cm.
- The small animal should be turned over mid way through the irradiation to have a better dose uniformity through the animal depth. Only one animal at a time should be irradiated to get a dose uniformity of less than 10%.

6.5 Future Work

The irradiator can be used also for partial animal body irradiation, where one can make a collimator to irradiate a specific organ of small animals like mice or even medium sizes animal like monkeys. However, careful dosimetric measurements using films or thermoluminescent dosimeters (TLDs) should be carried out as the scatter conditions can

make such measurements tricky depending on the size and location of the surrounding tissues.

The low quality, non-penetrative beams generated by the Faxitron can be used to irradiate only the skin of a small animal to induce skin cancer for research studies. Characterizing such a low quality beam probably requires a stable energy-response dosimeter and accurate determination of half-value layer.

A Monte Carlo model of the Faxitron CP160 X-ray irradiator can be developed to be used for dose distribution calculations inside small animals, with the help of imaging modalities such as small animal PET or CT scanners, and to investigate the dose delivered to different organs such as bones and lungs. Developing a good Monte Carlo model requires detailed knowledge of the dimensions and materials of the X-ray tube.

Bibliography

"Central axis depth dose data for use in radiotherapy, BJR Supplement no. 5", Br. J. Radiol, (1953).

"Central axis depth dose data for use in radiotherapy, BJR Supplement no. 10", Br. J. Radiol, (1961).

"Central axis depth dose data for use in radiotherapy, BJR Supplement no. 11", Br. J. Radiol, (1972).

"Central axis depth dose data for use in radiotherapy, BJR Supplement no. 17", Br. J. Radiol, (1983).

"Central axis depth dose data for use in radiotherapy, BJR Supplement no. 25", Br. J. Radiol, (1996).

P. Andreo, D. T. Burns, K. Hohlfeld et al., *Absorbed Dose Determination in External Beam Radiotherapy: An International Code of Practice for Dosimetry Based on Standards of Absorbed Dose to Water; Technical Reports Series No. 398.* (International Atomic Energy Agency, Vienna, 2000).

P. Andreo, J.C. Cunningham, K Hohlfeld et al., *Absorbed dose determination in photon and electron beams: an international code of practice, IAEA Technical Reports Series 277.* (International Atomic Energy Agency, Vienna, 1987).

M. Boutillon and A. M. Perroche-Roux, "Re-evaluation of the *W* value for electrons in dry air", Phys Med Biol **32**, 213-219 (1987).

M. J. Butson, T. Cheung, and P. K. Yu, "Weak energy dependence of EBT gafchromic film dose response in the 50 kVp-10 MVp X-ray range", Appl Radiat Isot **64** (1), 60-62 (2006).

Faxitron X-ray Corporation, *43855F Cabinet X-ray System Technical Manual, CP160 Option*

S. Devic, J. Seuntjens, E. Sham et al., "Precise radiochromic film dosimetry using a flat-bed document scanner", Med Phys **32** (7), 2245-2253 (2005).

NCS (Netherlands Commission on Radiation Dosimetry), *Dosimetry for low and medium energy x-rays: a code of practice in radiotherapy and radiobiology, NCS Report no. 10.* (NCS, Delft, The Netherlands, 1997).

R. Gastorf, L. Humphries, and M. Rozenfeld, "Cylindrical chamber dimensions and the corresponding values of A_{wall} and $N_{gas}/(N_x A_{ion})$", Med Phys **13** (5), 751-754 (1986).

J. H. Hubbell and S. M. Seltzer, Tables of X-Ray Mass Attenuation Coefficients and Mass Energy-Absorption Coefficients from 1 keV to 20 MeV for Elements Z = 1 to 92 and 48 Additional Substances of Dosimetric Interest NISTIR 5632. National Institute of Standards and Technology (NIST).

H. E. Johns and J. R. Cunningham, *The Physics of Radiology*, 4th ed. (Thomas, Springfield, Ill., 1983).

F. M. Khan, *The Physics of Radiation Therapy*, 3rd ed. (Lippincott Williams & Wilkins, Philadelphia ; London, 2003).

S. C. Klevenhagen, "Experimentally determined backscatter factors for x-rays generated at voltages between 16 and 140 kV", Phys Med Biol **34**, 1871-1882 (1989).

S. C. Klevenhagen, R. J. Aukett, R. M. Harrison et al., "The IPEMB code of practice for the determination of absorbed dose for x-rays below 300 kV generating potential (0.035 mm Al-4 mm Cu HVL; 10-300 kV generating potential)." Phys Med Biol **41** (12), 2605-2625 (1996).

R. T. Knight and A. E. Nahum, "Depth and field-size dependence of ratios of mass-energy-absorption coefficient, water-to-air, for kV X-ray dosimetry", *in Proceedings of the of the IAEA International Symposium on Measurement Assurance in Dosimetry*, edited by IAEA, Vienna, 1994)

C. M. Ma, C. W. Coffey, L. A. DeWerd et al., "AAPM protocol for 40-300 kV x-ray beam dosimetry in radiotherapy and radiobiology", Med Phys **28** (6), 868-893 (2001).

C. M. Ma and A. E. Nahum, "Calculations of ion chamber displacement effect corrections for medium-energy x-ray dosimetry", Phys Med Biol **40** (1), 45-62 (1995).

C. M. Ma and A. E. Nahum, "Monte Carlo calculated correction factors for a NE2571 chamber in medium-energy photon beams", *in Proceedings of the IAEA International Symposium on Measurement Assurance in Dosimetry*, edited by IAEA, Vienna, 1994)

C. M. Ma and A. E. Nahum, "Monte Carlo calculated stem effect correction for NE2561 and NE2571 chambers in medium-energy x-ray beams", Phys Med Biol **40** (1), 63-72 (1995).

C. M. Ma and J. P. Seuntjens, "Correction factors for water-proofing sleeves in kilovoltage x-ray beams", Med Phys **24** (9), 1507-1513 (1997).

C. M. Ma and J. P. Seuntjens, "Mass-energy absorption coefficient and backscatter factor ratios for kilovoltage x-ray beams", Phys Med Biol **44** (1), 131-143 (1999).

ICRU (International Commission for Radiation Units and Measurements), *Fundamental Quantities and Units for Ionizing Radiation, ICRU Report No. 60.* (1998).

ICRU (International Commission for Radiation Units and Measurements), *Radiation dosimetry: Measurement of absorbed dose in a phantom irradiated by a single beam of x- or gamma rays, ICRU Report No. 23.* (1973).

A. E. Nahum,"kV X-ray Dosimetry: Current Status and Future Challenges (AAPM Proc. no 11)", *in Proceedings of the Kilovoltage X-ray Beam Dosimetry for Radiotherapy and Radiobiology*, edited by C.M. Ma and Jan P. Seuntjens (Medical Physics Publishing, Madison, Wisconsin, 1998)

DIN (Deutsch Institut Fur Normung), *Klinische Dosimetrie: anwendung von Röntgenstrahlen mit Röhrenspannungen von 100 bis 400 kV in der Strahlentherapie* (DIN, Berlin, 1996).

C. G. Orton and J. B. Seibert, "The measurement of teletherapy unit timer errors", Phys Med Biol **17** (2), 198-205 (1972).

E. B. Podgorsak (Editor), *Radiation Oncology Physics : A Handbook for Teachers and Students*. (International Atomic Energy Agency, Vienna, 2005).

J. Seuntjens, H. Thierens, and U. Schneider, "Correction factors for a cylindrical chamber used in medium-energy x-ray beams", Phys. Med. Biol. **38**, 805-832 (1993).

J. Seuntjens and F. Verhaegen, "Dependence of overall correction factor of a cylindrical ionization chamber on field size and depth in medium-energy x-ray beams", Med Phys **23** (10), 1789-1796 (1996).

R. C. Tailor, W. F. Hanson, N. Wells et al., "Consistency of absorbed dose to water measurements using 21 ion-chamber models following the AAPM TG51 and TG21 calibration protocols", Med Phys **33** (6), 1818-1828 (2006).

I. Tannock, *The Basic Science of Oncology*, 4th ed. (McGraw-Hill, Medical Pub. Division, New York, 2005).

J. E. Turner, *Atoms, Radiation, and Radiation Protection*, 2nd ed. (J. Wiley, New York, 1995).

M. S. Weinhous and J. A. Meli, "Determining P_{ion}, the correction factor for recombination losses in an ionization chamber", Med Phys **11** (6), 846-849 (1984).

J. Zoetelief, J. J. Broerse, R. W. Davies et al., "Protocol for X-ray dosimetry in radiobiology", Int J Radiat Biol **77** (7), 817-835 (2001).